ISSN 1063-7796, Physics of Particles and Nuclei, 2011, Vol. 42, No. 2, pp. 215–250. © Pleiades Publishing, Ltd., 2011.
Original Russian Text © I.A. Pshenichnov, 2011, published in Fizika Elementarnykh Chastits i Atomnogo Yadra, 2011, Vol. 42, No. 2.

Electromagnetic Excitation and Fragmentation of Ultrarelativistic Nuclei

I. A. Pshenichnov

Institute for Nuclear Research, Russian Academy of Sciences, Moscow, 117312 Russia

Abstract—Electromagnetic interactions of high-energy nuclei in ultraperipheral collisions are considered. Such collisions, which take place without any overlap of nuclear densities, can be considered as irradiation of nuclei by intense photon beams with a broad energy spectrum. This leads to several unusual phenomena, such as mutual electromagnetic excitation of nuclei, including exotic double and triple excitations of giant resonances, and multifragmentation of nuclei. The RELDIS model is presented, which describes fragmentation of nuclei and meson production by equivalent photons. It is shown that the RHIC and LHC colliders provide unique opportunities to study electromagnetic interactions of ultrarelativistic nuclei. The cross sections calculated by the RELDIS model are used in the method of monitoring the LHC luminosity on the basis of neutron emission rates, as well as to simulate interactions of beam nuclei with LHC construction elements.

DOI: 10.1134/S1063779611020067

CONTENTS

1. INTRODUCTION

True scientists always search for new, unusual properties of objects or phenomena to be discovered under extreme conditions. A superhigh energy nucleus-nucleus collider, the Relativistic Heavy Ion Collider (RHIC) [1] at the Brookhaven National Laboratory (BNL, United States), was constructed to study the behavior of nuclear matter under extreme conditions. A number of important scientific results considered, in particular, in recently published reviews [2–4] have been obtained in experiments on nucleus–nucleus collisions conducted at the RHIC.

At the time of writing this paper, the construction of another unique accelerator, the Large Hadron Collider (LHC) [5] at the Conseil Européen pour la Recherche Nucléaire (CERN, Geneva), has been completed. The collider will make possible studies of the proton–proton and nucleus–nucleus interactions at the unprecedented energies of colliding beams.

The highest expectations are associated with central or close-to-central nuclear collisions, i.e., events with large overlap of nuclear densities, and with the search for quark–gluon plasma in such events. The RHIC and LHC accelerators make it possible to reach record-breaking energy densities of ~10–100 GeV/fm^3 in central nuclear collisions and create conditions for the phase transition predicted by theorists from hadronic matter to quark–gluon plasma [2, 3, 6, 7]—a peculiar state of matter in which our Universe is supposed to have existed during the first moments of its formation.

Comparison of various quantities measured in central events with analogous ones measured in peripheral collisions may provide compelling evidence in favor of the phase transition. This involves sorting events according to their degree of "centrality"[1] or to the impact parameter b, which is directly related to event characteristics in the context of various theoretical models. Such characteristics can be measured in an experiment by using detectors in combination that determine the multiplicity of produced hadrons and spectator neutrons. The latter are emitted in the forward direction by relatively cold nuclear fragments located outside the region of overlap of the nuclei. There are dedicated detectors, zero degree calorimeters (ZDCs), that determine the number of spectator nucleons. In the experiments at the RHIC [8], ZDCs allow detecting neutrons only, while in the forthcoming experiments at the LHC [9, 10], they will provide a means of registering both neutrons and protons.

The physics programs of the experiments at the RHIC and LHC colliders are mainly focused on studying nuclear collisions in which strong interactions of nuclear constituents and produced hadrons dominate. However, ultraperipheral nuclear collisions outside the region of hadronic interactions [4, 11–14] have also actively been discussed in recent decades. This is the region of "centrality" where no geometrical overlap of nuclear densities occurs: $b \geq R_1 + R_2$, where R_1 and R_2 are radii of colliding nuclei, and electromagnetic[2] excitation of nuclei is the concern [15]. The nuclei appear to be spectators with respect to hadronic interactions, but they can be disintegrated by electromagnetic forces exerted by the Lorentz-contracted Coulomb fields of nuclei. Note that, in order to study electromagnetic interactions of nuclei one can use ZDC calorimeters, which have already been constructed and will be used in experiments in combination with detectors that are intended to detect products of hadronic interactions at large angles.

The study of electromagnetic interactions of relativistic nuclei is of both fundamental and practical importance. Getting down to the fundamental aspect of the problem, it should be noted that, for many decades, it has been the study of interactions of electrons and photons with nuclei that yielded unique information about the size and structure of the latter, as well as the properties of giant resonances viewed as collective excitations [16–18]. Analysis of deep inelastic scattering of electrons off protons and nuclei gave the key to understanding their partonic structure [19]. The method of tagged photons is currently widely used in experiments studying meson photoproduction on nuclei [20]. The success of all such studies was largely related to the completeness of quantum electrodynamics as a theory of electromagnetic processes, which, in particular, provides a quantitative description of the direct mechanism of nuclear photoexcitation or initial interaction of a lepton with nucleons or partons. All these simplify interpretation of the strong interaction processes that take place at the second stage of photonuclear reactions.

Thus, electron accelerators and photon sources operating on the base of the former are important tools for fundamental nuclear physics research. In these cases accelerated electrons with unit charges $1e$ are used. On the other hand, relativistic heavy nuclei with large charges can even more be thought of as intense photon sources with a broad spectrum [11–13], so-called "photon factories."

Electromagnetic excitation of nuclei in collisions at intermediate energies (the Lorentz factor of incoming nucleus $\gamma \sim 1$) allows studying reactions inverse to nucleosynthesis [21] and double giant resonances [22–24]. For secondary beams of exotic unstable nuclei, electromagnetic excitation is one of the few ways to examine their nuclear structure [25]—in particular, the fissility of unstable nuclei [26]—since a standard target to be irradiated by electrons and photons cannot be prepared out of such nuclei.

The intensity of the virtual photon flux generated by a moving nucleus with a charge Ze is associated with both a coherent effect of all Z charges of protons and Lorentz contraction of their Coulomb fields. Therefore, the task of studying the behavior of nuclei in superstrong electromagnetic fields acquires an independent fundamental importance exactly for ultrarelativistic energies of colliding nuclei, $\gamma \gg 1$. Indeed, a simple estimate shows[3] that, at the moment when nuclei are closest to each other, the potential of the Lorentz-contracted Coulomb field $V_c \sim \alpha\gamma Z/b$, where α is the fine structure constant, can considerably exceed the total binding energy of a partner-nucleus ~1 GeV. Using the values typical of ultrarelativistic heavy nuclei for $\gamma \gg \alpha^{-1}$, $Z \sim 50$, and the impact parameter $b \sim 10$ fm, we obtain for $V_c \sim \alpha\gamma$ GeV $\gg 1$ GeV. Here both the large Z and Lorentz-factor $\gamma \gg 1$ values are crucial; therefore, one can expect, for instance, a partner-nucleus to explosively disintegrate (a multifragmentation process [27])

[1] It is difficult to translate the term "centrality" used in English articles into Russian.

[2] At nonrelativistic energies the term "Coulomb excitation" is used more often.

[3] Hereafter, the natural system of units is used, in which $\hbar = c = 1$.

among other mechanisms of its breakup. As will be shown below, along with the most probable low-energy nuclear excitations, high-energy ones become possible only at ultrarelativistic energies. In addition, electromagnetic excitation of nuclei at colliders can serve as a unique tool to study nuclear structure, in particular, multiphoton excitations of nuclei and other phenomena unobservable in fixed-target experiments at low and intermediate energies. On the other hand, unlike electro- and photoreactions, electromagnetic dissociation of nuclei occurs under the impact of partner-nuclei also experiencing hadronic collisions. This is why it is necessary to reliably distinguish in experiment electromagnetic and hadronic collisions, and introduce in theoretical considerations of electromagnetic collisions a correction for the strong absorption.

Interest in electromagnetic interactions of relativistic nuclei at colliders is also related with a number of practical problems. First, electromagnetic interactions of nuclei, along with hadronic ones, lead to a nucleon loss by nuclei, i.e., change in nuclear charge, mass, and, consequently, trajectories of nuclei in the collider magnetic field. Since the total cross section of electromagnetic interaction at the collider energies considerably exceeds that of hadronic interaction of nuclei, it is the electromagnetic interaction that largely determines the beam lifetime at such accelerators [28]. Second, the products of electromagnetic dissociation—nuclear fragments—can cause exposure to radiation and create heat load in construction elements of the collider [29]. Also, an up-to-date model of electromagnetic dissociation of nuclei capable of predicting various characteristics of such processes is necessary for dealing with the practical problems listed.

In this paper the results obtained with the Relativistic Electromagnetic Dissociation (RELDIS) model of electromagnetic dissociation of nuclei specifically developed to describe fragmentation of ultrarelativistic nuclei under the impact of intense electromagnetic fields are presented. Formulation of the model, summarization of its main results, and their comparison with experimental data have been presented in the past in a series of papers (see, in particular, [14, 30–32]). It is in recent years that studies of electromagnetic dissociation of ultrarelativistic nuclei have become of particular interest in connection with the new experimental results obtained on electromagnetic interactions of nuclei at the RHIC, as well as with intense preparation for nucleus–nucleus collisions to be soon studied at the LHC. That is why the purpose of this paper is to review, in retrospect, the RELDIS results, with the main emphasis placed on the processes of mutual electromagnetic dissociation of heavy nuclei (gold and lead) at the RHIC and LHC colliders. Such nuclei have cross sections of electromagnetic dissociation substantially exceeding those that correspond to their strong interactions. However, ultraperipheral interactions are characterized by considerably lower particle multiplicity produced in a single event.

In Section 2, the Weizsäcker–Williams method of equivalent photons is presented as applied to ultraperipheral collisions of nuclei. Implementation of this method in the RELDIS model to simulate interactions of equivalent photons with nuclei by using the Monte Carlo method is described. Section 3 is devoted to consideration, in the framework of the RELDIS model, of the electromagnetic dissociation of accelerated nuclei interacting with fixed targets that leads, in particular, to neutron emission by nuclei. Specific electromagnetic processes resulting in an increase of nuclear charge are shown to be probable. In all these cases, the state into which a partner-nucleus falls after collision is not studied. Mutual electromagnetic dissociation of relativistic nuclei is considered in Section 4. Detection of the states of both collision partners in ultraperipheral collisions is only possible with colliding beams of nuclei. This makes it possible to select events with mutual electromagnetic dissociation. It is shown that relatively small values of the impact parameters correspond to such events. It is demonstrated that mutual electromagnetic dissociation at ultrarelativistic energies opens up new opportunities to study multiphoton electromagnetic excitations of nuclei, in particular, triple excitations of giant resonances in nuclei. Application of the model results to monitoring the RHIC and LHC luminosities is dealt with in Section 5.

2. THE WEIZSÄCKER–WILLIAMS METHOD: EQUIVALENT PHOTONS AND THEIR ABSORPTION BY NUCLEI

2.1. The Weizsäcker–Williams Method

Let us consider ultraperipheral collisions of accelerated nuclei (see Fig. 1). The mass numbers and charges of colliding nuclei are denoted as A_1, A_2, and Z_1, Z_2, respectively. The term "ultraperipheral collisions" is applicable to electromagnetic interactions of nuclei with impact parameters b exceeding the sum of their radii: $b > R_1 + R_2$. Such collisions can be observed in the interactions of accelerated nuclei with a fixed target, as well as at nucleus–nucleus colliders. We emphasize that ultraperipheral collisions should be distinguished from peripheral nuclear collisions with $b \simeq R_1 + R_2$ that occur due to the strong interactions.

In both cases, while considering the result of interaction with respect to, say, the nucleus A_2, it is convenient to assume it to be a target nucleus and proceed to its rest frame, as is diagrammatically shown in Fig. 1. Using the Weizsäcker–Williams method [33], the impact of the Lorentz-contracted Coulomb field of the nucleus A_1 on the nucleus A_2 can be considered as an absorption of one or several equivalent photons by the nucleus A_2 (see Fig. 1). The method of equivalent photons was proposed by Fermi [34, 35], who was first

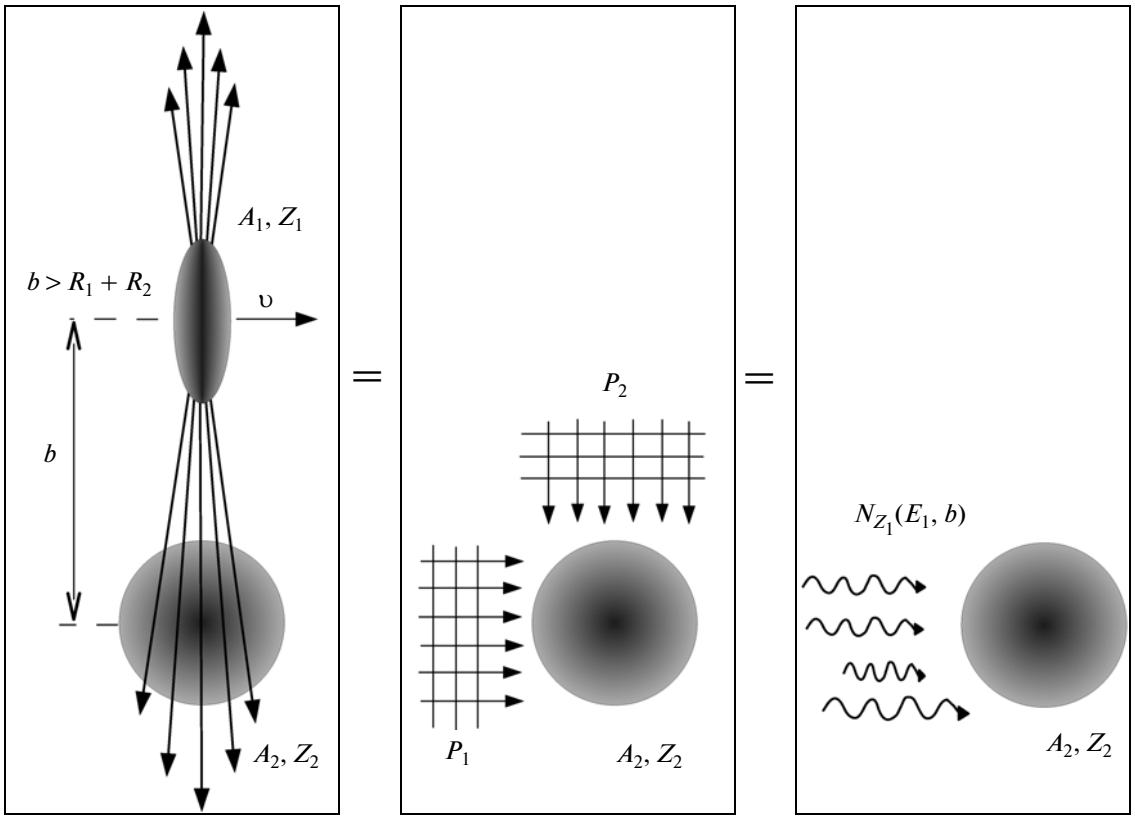

Fig. 1. In ultraperipheral collisions the nuclei (A_1, Z_1) and (A_2, Z_2) act on each other by their electromagnetic fields. Following the Weizsäcker–Williams method, such an impact on the partner (A_2, Z_2) can be considered as being equivalent to absorbing by the latter the electromagnetic momenta P_1 and P_2 from the nucleus (A_1, Z_1), represented by the spectrum of equivalent photons $N_{Z_1}(E_1, b)$, which depends on the value of the impact parameter b.

to represent the field of a moving charge as a photon flux in his attempt at solving the problem of interactions between charged particles and nuclei. In works by Weizsäcker [36] and Williams [37], such an approach was further applied to calculating the interactions of fast electrons and protons with matter.

The justification of the Weizsäcker–Williams method within the framework of quantum electrodynamics has long been included in textbooks (see, for example, [33]). Additionally, the reviews already mentioned [11–13, 15] contain a detailed derivation of the basic relations of this method carried out by using quantum mechanics in both nonrelativistic and relativistic cases. Here we shall only give a derivation of the expression for the spectrum of equivalent photons $N_{Z_1}(E_1, b)$ following [15, 33]. Special attention will be paid to the spectrum boundaries, and the peculiarities of its shape will be discussed.

Let us assume that emission and absorption of equivalent photons do not affect the motion of nuclei participating in these processes in a significant way. This assumption will be verified later on; for now, it will let us assume that the nucleus A_1 before and after a collision moves in a straight line along the z axis with a velocity υ (see Fig. 1). Then, the nucleus A_2 being at rest and sitting at the origin of the coordinate system feels electric $\vec{E}_t$, E_z and magnetic $\vec{B}_t$, B_z fields, which vary with time t, in the directions transverse to and along the z axis, respectively:

$$\vec{E}_t = \frac{-Z_1 e\gamma \vec{b}}{(b^2 + \gamma^2 \upsilon^2 t^2)^{3/2}}, \quad \vec{B}_t = \frac{\vec{\upsilon}}{c} \times \vec{E}_t, \tag{1}$$

$$E_z = \frac{-Z_1 e\gamma \upsilon t}{(b^2 + \gamma^2 \upsilon^2 t^2)^{3/2}}, \quad B_z = 0. \tag{2}$$

Here $\gamma = (1 - \beta^2)^{-1/2}$ denotes the Lorentz factor of the A_1 nucleus with the velocity $\beta = \upsilon/c$ in terms of the speed of light c. If each of the colliding nuclear beams has a Lorentz factor γ_{beam} in the laboratory frame, then, in the rest frame of one of the nuclei, another nucleus has the Lorentz factor $\gamma = 2\gamma_{\text{beam}}^2 - 1$. For example, $\gamma = 1.7 \times 10^7$ for nuclei colliding at the LHC. To grasp the scale of the Lorentz-contraction of the Coulomb field in this case, it should be remarked that such a contraction of the observed longitudinal

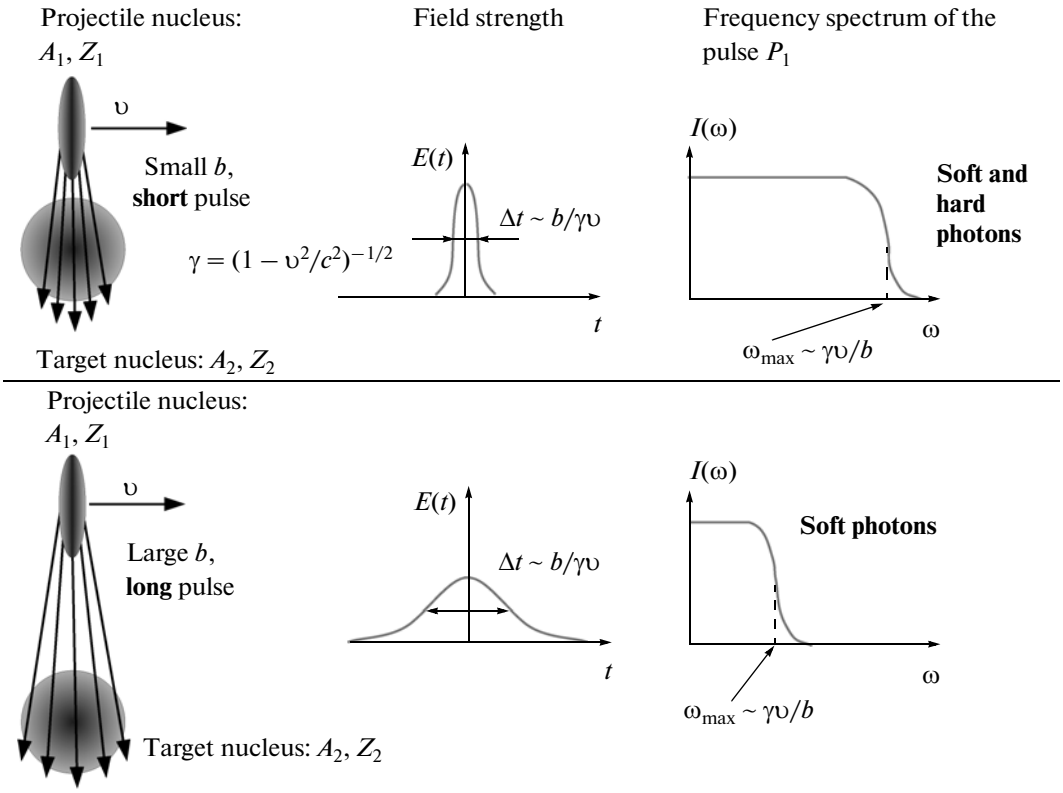

Fig. 2. Comparison of spectra of equivalent photons in ultraperipheral collisions for large and small values of the impact parameter b.

dimensions of an ultrarelativistic object roughly corresponds to the length of a train consisting of several tens of cars contracted to the thickness of a sheet of paper.

In the collisions of ultrarelativistic nuclei at $\gamma \gg 1$, the fields in (1) and (2) act within a rather short time $\Delta t \sim b/\gamma c$ and are equivalent to the two plane wave radiation pulses P_1 and P_2 (see Fig. 1). Strictly speaking, representing the pulse P_2 as a plane wave requires a presence of the respective magnetic field $B_z = \upsilon E_z/c$ instead of $B_z = 0$ in Eq. (2). It will be shown below that the contribution of P_2 turns out to be negligibly small at the ultrarelativistic energies of nuclei in which we are interested. Therefore, this simplification is valid.

The amount of energy absorbed by the nucleus (A_2, Z_2) per unit area of its cross section and per unit of a frequency interval is found by calculating the Fourier-expansions $\vec{E}(\omega)$ and $\vec{B}(\omega)$ of the corresponding electric and magnetic fields:

$$I(\omega, b) = \frac{c}{4\pi}\left|\vec{E}(\omega) \times \vec{B}(\omega)\right|. \qquad (3)$$

This allows a number of equivalent photons $N(E, b)$ to be evaluated with a given energy $E = \hbar\omega$ by using the relation $I(\omega, b)d\omega = \hbar\omega N(\hbar\omega, b)d(\hbar\omega)$.

The calculations result in the energy spectrum of equivalent photons from a partner-nucleus A_1. This latter spectrum is written in the rest frame of A_2 nucleus as follows:

$$N_{Z_1}(E_1, b) = \frac{\alpha Z_1^2}{\pi^2}\frac{x^2}{\beta^2 E_1 b^2} \times \left(K_1^2(x) + \frac{1}{\gamma^2}K_0^2(x)\right). \qquad (4)$$

Here α denotes the fine structure constant and the quantity $x = \omega b/\gamma\upsilon = E_1 b/\gamma\beta\hbar c$ stands for an argument of the modified Bessel function of zero and first orders K_0 and K_1, respectively. The second term corresponding to the pulse P_2 enters with a factor of $1/\gamma^2$ and, therefore, contributes insignificantly at ultrarelativistic energies for $\gamma \gg 1$. Consequently, both $I(\omega, b)$ and, respectively, $N_{Z_1}(E_1, b)$ are solely determined by the pulse P_1 and written in terms of the dimensionless function $x^2K_1^2(x)$, which is shaped as a steplike one with a smooth boundary (see Fig. 2). The upper limit of the spectrum is fixed by the energy corresponding to the value $x = 1$ and is equal to $E_1^{max} = \gamma\beta/b$.

Indeed, the duration of the electromagnetic pulse from the Lorentz-contracted Coulomb field, which exerts an impact upon a partner-nucleus, is propor-

tional to the distance from a nucleus-emitter: $\Delta t \sim b/\gamma\upsilon$ (see Fig. 2). As a result, for small impact parameters b, the Fourier transforms of the electric field pulses give a broad spectrum of equivalent photons that includes frequencies up to $\omega_{max} \sim 1/\Delta t = \gamma v/b$, and, respectively, both soft and hard photons. Quite to the contrary, collisions with large impact parameters b are characterized by a narrow spectrum represented only by soft photons. Since integration over the impact parameter taking into account the $2\pi bdb$ factor leads to a significant contribution of collisions with large b, one can expect relatively soft photons to dominate in ultraperipheral interactions. Thus, while considering ultraperipheral collisions without selecting events by the impact parameter, the nuclei can be thought of as exchanging mostly low-energy photons.

Since a moving relativistic nucleus emits photons as a whole, such a coherence condition restricts the energies and transverse momenta of equivalent photons. We denote the initial and final four-momenta of a nucleus, which emits a photon, with $P_i^\mu = (E_i, \vec{p}_i)$ and $P_f^\mu = (E_f, \vec{p}_f)$. In a nucleus the proton charges concentrate in the region with a radius R; therefore, the coherence condition $Q^2R^2 \le 1$ constrains the square of four-momentum carried away by a photon $Q^\mu = P_f^\mu - P_i^\mu$:

$$Q^2 \le 1/R^2. \tag{5}$$

Thus, the equivalent emission from accelerated nuclei is composed of photons with small virtuality; hence, photons can be considered to be real, unlike, e.g., those in the reactions (e, e').

We denote the photon four-momentum as $q^\mu = (E_\gamma, \vec{q}) = -Q^\mu$. We now estimate the photon energy E_γ and the component of its momentum $q_\perp$ transverse to the direction of motion of a nucleus. The condition for a nucleus to stay in its ground state after photon emission is written as $P_i^2 = P_f^2 = (P_i - q)^2$. From this we find

$$q^2 = 2P_iq = 2E_i\left(E_\gamma - \frac{\vec{p}_i\vec{q}}{E_i}\right) = 2E_i(E_\gamma - \beta q_\parallel), \tag{6}$$

where $\beta = \vec{p}_i/E_i$ and $q_\parallel$ denotes the longitudinal component. An ultrarelativistic nucleus possesses considerable kinetic energy and a photon emission does not alter it either; therefore, $q^2/2E_i \approx 0$ and, respectively,

$$q_\parallel \approx \frac{E_\gamma}{\beta}. \tag{7}$$

Substituting this estimate into the expression for Q^2, we obtain

$$\begin{aligned} Q^2 &= -q^2 = -E_\gamma^2 + \vec{q}_\perp^{\,2} + \vec{q}_\parallel^{\,2} \\ &\approx -E_\gamma^2 + \vec{q}_\perp^{\,2} + \frac{E_\gamma^2}{\beta^2} \approx \frac{E_\gamma^2}{\gamma^2\beta^2} + \vec{q}_\perp^{\,2}. \end{aligned} \tag{8}$$

For $\gamma \gg 1$ and $\beta \approx 1$ and using Eq. (5), we derive (see [13])

$$q_\parallel \approx E_\gamma < \frac{\gamma}{R}, \tag{9}$$

$$q_\perp < \frac{1}{R}. \tag{10}$$

Such a constraint imposed on E_γ is consistent with the estimate of maximal photon energy obtained by calculating the collision time at a given b, since $b_{min} \simeq R$. From constraint (10) it follows that the quantity $q_\perp$ is negligibly small, and this is compatible with the possibility of neglecting the contribution coming from the pulse P_2 for $\gamma \gg 1$ that has just been discussed. Thus, it can be assumed that the wave vector of equivalent photon is along the direction of motion of ultrarelativistic nucleus emitting the photon.

2.2. Photon Absorption by Nuclei in the Intranuclear Cascade Model

As shown above, the Weizsäcker–Williams method takes the Coulomb field of an accelerated nucleus to be equivalent to a photon flux with the specific broad spectrum presented in (4). An ultraperipheral interaction between accelerated and target nuclei will be viewed as an absorption of equivalent photons by the latter. In this section we shall actually consider a procedure simulating photon–nucleus interactions—the cascade model of photonuclear reactions that underlies the RELDIS model.

The wavelength $\lambda\!\!\!^{-}$ of a photon interacting with a nucleus determines the basic properties of this interaction. At the photon energy $E_\gamma \le 40$ MeV, the wavelength $\lambda\!\!\!^{-}$ is comparable to the size of a nucleus and the excitation of a nucleus as a whole in the form of a giant dipole resonance (GDR) is the most probable photoabsorption process to take place within this energy interval. The electromagnetic field of a photon causes all the protons of a nucleus to coherently oscillate about neutrons. Within the energy interval $40 \le E_\gamma \le 140$ MeV (below the pion photoproduction threshold), $\lambda\!\!\!^{-}$ turns out to be comparable to the internucleon distance in a nucleus, thus allowing for photon absorption by the quasi-deuteron proton–neutron pairs in a nucleus. Finally, for $E_\gamma \ge 140$ MeV, $\lambda\!\!\!^{-}$ becomes less than a nucleon radius and hadron photoproduction occurs on individual constituent nucleons.

A modern version of the intranuclear cascade model (INC) for the photonuclear reactions that takes into account the diversity of the processes considered above is presented in [38–40], where predictions of this model are compared with various experimental data on absorption of real photons by nuclei. Earlier versions of INC (see, in particular, [41]) could be employed for the calculations only below the two-pion photoproduction threshold. Part of the photon energy absorbed by a nucleus is transferred to the fast particles (nucleons and mesons) leaving a nucleus [38, 40] during intranuclear cascade evolution, while the remainder turns into the excitation energy E^* of a nuclear system, the so-called residual nucleus.

Once the last fast particle has left a residual nucleus, its evolution can be described within a statistical approach that assumes the onset of thermal equilibrium in a residual nucleus. Such an assumption is justified by the intense interactions among nucleons of a residual nucleus, thus promoting establishment of thermal equilibrium. As demonstrated by numerous experiments and described generally by the statistical model SMM (see [27, 42]), the branching ratios of nuclear fragmentation caused by virtual photons are largely determined by the excitation energy E^* of a residual nucleus.

Successive emission of nucleons or light clusters, for example, α-particles, which is called evaporation, dominates at excitation energies of a residual nucleus less than 3 MeV per nucleon. At energies above 4 MeV per nucleon, a process of simultaneous nuclear disintegration to three or more fragments, so-called nuclear multifragmentation, starts to dominate. Within the energy interval from 3 to 4 MeV per nucleon both processes coexist. In addition, a heavy residual nucleus can undergo fission into two nuclear fragments [39] even at small excitation energies.

Following [31], let us consider a change in both the excitation energy of a residual nucleus E^* and the nature of the photonuclear reaction with increasing photon energy E_γ. The fraction of E_γ, which on average goes to E^*, as well as the mean value of E^* per nucleon of a residual nucleus, are displayed in Fig. 3 as a function of E_γ. Photoabsorption by heavy gold Au and lead Pb nuclei is considered as an example. The mean values for a Pb nucleus are given in Figs. 3a and 3b.

If photons are absorbed in the vicinity of giant resonance (GR), $6 \le E_\gamma \le 30$ MeV, their energies completely transform into the excitation energy of a nucleus E^*. Deexcitation of preactinide nuclei, such as Au and Pb with fission thresholds exceeding 30 MeV, proceeds mainly through neutron evaporation, since the energies of neutron separation are about 7 MeV. Because of a high Coulomb barrier in heavy nuclei, proton emission is considerably suppressed in the vicinity of GR.

A detailed experimental investigation of the reactions (γ, n), (γ, $2n$), (γ, $3n$), and (γ, $4n$) on the nuclei

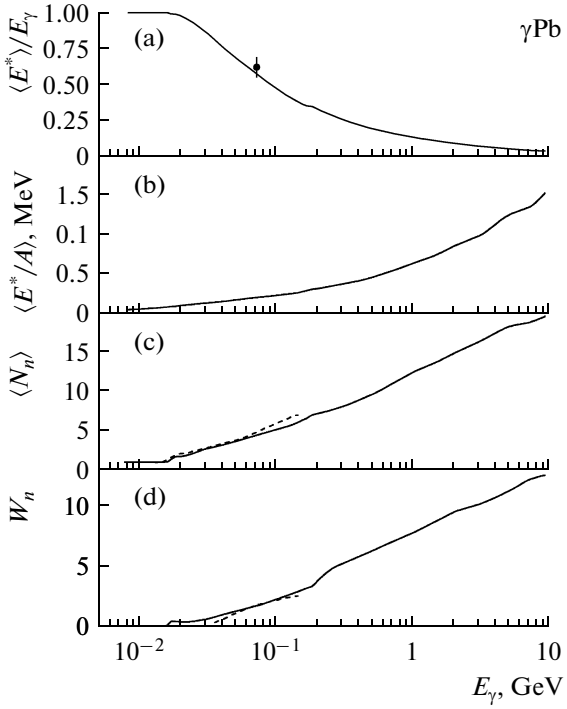

Fig. 3. (a) Ratio of the mean excitation energy of a residual nucleus $\langle E^*\rangle$ to the energy of a photon E_γ absorbed by a nucleus, (b) mean values E^* per nucleon of a residual nucleus, (c) mean values of the photoneutron multiplicity $\langle N_n\rangle$, and (d) width of the neutron multiplicity distribution $W_n = \sqrt{\langle N_n^2\rangle - \langle N_n\rangle^2}$ as a function of E_γ in photoabsorption on a lead nucleus [31]. Solid curves correspond to the RELDIS model results; the dashed ones and data point represent experimental data [48].

^{197}Au and ^{208}Pb in the vicinity of GR is presented in [43]. The registration of the reaction (γ, $4n$) means that a nucleus can acquire an excitation energy E^* that reaches 30 MeV. In order to simulate particle emission in the vicinity of GR, let us assume that a nucleus with $E^* = E_\gamma$ is produced and use the Weisskopf evaporation model, which is a part of SMM [42].

Starting from $E_\gamma = 30$ MeV, the quasi-deuteron mechanism of photoabsorption becomes important, which dominates all the way up to the pion production threshold $E_\gamma = 140$ MeV. On average, only a fraction of the photon energy transforms into the excitation energy of a residual nucleus E^*, while the remainder is carried away by the fast nucleons that constitute a quasi-deuteron pair that absorbed a photon.

The corresponding cross section of the two-nucleon photoabsorption by a heavy nucleus σ_A is determined by using the Levinger quasi-deuteron model [44] further developed in [45]:

$$\sigma_A^{\mathrm{QD}} = kZ(1 - Z/A)\sigma_d^{\mathrm{exch}}. \qquad (11)$$

Table 1. Meson photoproduction channels on intranuclear nucleons taken into account by the intranuclear cascade model [38] used in the RELDIS model

γp-interaction	γn-interaction
$\gamma p \longrightarrow \pi^+ n$	$\gamma n \longrightarrow \pi^- p$
$\gamma p \longrightarrow \pi^0 p$	$\gamma n \longrightarrow \pi^0 n$
$\gamma p \longrightarrow \pi^- \Delta^{++}$	$\gamma n \longrightarrow \pi^- \Delta^+$
$\gamma p \longrightarrow \pi^0 \Delta^+$	$\gamma n \longrightarrow \pi^0 \Delta^0$
$\gamma p \longrightarrow \pi^+ \Delta^0$	$\gamma n \longrightarrow \pi^+ \Delta^-$
$\gamma p \longrightarrow \eta p$	$\gamma n \longrightarrow \eta n$
$\gamma p \longrightarrow \omega p$	$\gamma n \longrightarrow \omega n$
$\gamma p \longrightarrow \rho^0 p$	$\gamma n \longrightarrow \rho^0 n$
$\gamma p \longrightarrow \rho^+ p$	$\gamma n \longrightarrow \rho^- p$
$\gamma p \longrightarrow \pi^+ \pi^- p$	$\gamma n \longrightarrow \pi^+ \pi^- n$
$\gamma p \longrightarrow \pi^0 \pi^+ n$	$\gamma n \longrightarrow \pi^0 \pi^- p$
$\gamma p \longrightarrow \pi^0 \pi^0 \pi^0 p$	$\gamma n \longrightarrow \pi^0 \pi^0 \pi^0 n$
$\gamma p \longrightarrow \pi^+ \pi^- \pi^0 p$	$\gamma n \longrightarrow \pi^+ \pi^- \pi^0 n$
$\gamma p \longrightarrow \pi^+ \pi^0 \pi^0 n$	$\gamma n \longrightarrow \pi^- \pi^0 \pi^0 p$
$\gamma p \longrightarrow \pi^+ \pi^+ \pi^- n$	$\gamma n \longrightarrow \pi^+ \pi^- \pi^- p$
$\gamma p \longrightarrow i\pi N\ (4 \le i \le 8)$ in total 35 channels with four to eight pions	$\gamma n \longrightarrow i\pi N\ (4 \le i \le 8)$ in total 35 channels with four to eight pions

Here σ_d^{exch} denotes that part of the cross section of the deuteron photodisintegration reaction $\gamma d \longrightarrow np$ that proceeds through the meson exchange. This quantity was calculated in [46]. In Eq. (11) A and Z denote the mass number and charge of a nucleus that absorbs a photon and $k \approx 11$ [45] is the empiric factor.

It is convenient to calculate the nucleon angular distribution in the final state of the reaction $\gamma d \longrightarrow np$ by using the approximations of experimental data from [41]. Despite the fact that the cross section σ_d^{exch} rapidly falls off with increasing photon energy, the two-nucleon mechanism of a photoabsorption competes with the hadron photoproduction on an individual nucleon up to $E_\gamma \sim 0.5$ GeV.

The results of measurements presented in [45] show that a lead nucleus, which is excited after absorbing a photon with $30 \le E_\gamma \le 140$ MeV, can emit up to 12 neutrons. This observation gives an estimate of the mean excitation energy of such a nucleus: $\langle E_\gamma \rangle \le 70$–80 MeV. It was shown in [47], where one of the first versions of the intranuclear cascade model [41] was used, that the mean excitation energy of a residual nucleus $\langle E^* \rangle$ in photoabsorption processes on the nuclei ^{197}Au and ^{208}Pb for $30 \le E_\gamma \le 140$ MeV does not exceed 80 MeV. The results of the intranuclear cascade model used in RELDIS are also consistent with the experimental result mentioned (see Fig. 3). We also note that, in the energy interval E_γ under consideration, the fissility $\mathcal{P}_f$ of the nuclei ^{197}Au and ^{208}Pb is noticeable: $\mathcal{P}_f \sim 0.01$ and 0.1, respectively. Therefore, one can expect the neutron evaporation to compete with fission of those nuclei.

Above the pion photoproduction threshold at $E_\gamma \ge 140$ MeV, excitation of Δ-isobar on individual constituent nucleons dominates. Related to the latter, the effect of moderation in the $\langle E^* \rangle$ growth with increasing energy of an absorbed photon was noted in [47]. The results of calculations shown in Fig. 3a confirm this observation as well. Indeed, near the photoproduction threshold, the cross section of a secondary interaction of a produced slow pion with constituent nucleons is small. Having a high probability of leaving a nucleus without interaction, such a pion carries away a sizable fraction ($\approx m\pi$) of the photon energy. Only when the photon energy starts to increase and at $E_\gamma \approx 200$ MeV does the magnitude of $\langle E^* \rangle$ resume its growth, since the πN cross section sharply increases as the pion energy approaches the region of Δ-isobar excitation.

As calculations show, a heavy nucleus that absorbs a photon loses one or two nucleons during the fast cascade stage of the process and acquires the excitation energy $\langle E^* \rangle \sim 100$ MeV sufficient for vaporizing many neutrons or nuclear fission. The neutron evaporation takes place before or after fission, because the excited fission fragments can in their turn evaporate neutrons. Competition between evaporation and fission processes is described by the SMM [27].

Above the two-pion production threshold (at $E_\gamma \sim 400$ MeV), simulation of γN interaction becomes more complicated because of a large number of possible final states in the reaction. The partial cross sections of channels of γN interaction on constituent nucleons with meson production and the particle angular distributions in the final state of each of these channels will be described within the phenomenological approach given in [38], wherein both the two-body channels with baryon B^* and meson M^* resonances, $\gamma N \longrightarrow \pi B^*$ and $\gamma N \longrightarrow M^* N$, and nonresonant combinatorial contribution coming from the channels with a multiple meson production $\gamma N \longrightarrow i\pi N\ (2 \le i \le 8)$ are included. Such an approach deals with about 80 channels of multiple hadron photoproduction on a nucleon represented in Table 1.

When simulating a photonuclear reaction in the framework of INC, fast hadrons produced by the primary γN interaction initiate a cascade of secondary hadron–nucleon interactions on constituent nucleons. The multiple pion photoproduction becomes a

dominating process at a photon energy above several gigaelectronvolts.

The mean excitation energy of a residual nucleus was estimated in [48] to be $E^* = 43.4 \pm 5$ MeV from the experimental data on photoabsorption with $E_\gamma =$ 70 MeV obtained on a lead nucleus. As is shown in Fig. 3a, this value is in good agreement with INC predictions. In summary, we note that, with the photon energy increasing from the GR region up to a few gigaelectronvolts, the nature of Coulomb nuclear excitation evolves from excitations of collective states in nuclei (such as giant resonances) toward excitations of individual nucleon in a nucleus (a delta-isobar, other baryon resonances and a multiple meson production); see Fig. 3. In the latter case, up to 95% of the photon energy is released in the form of fast particles leaving a nucleus. Nonetheless, the remaining energy that transforms into excitation of a residual nucleus makes it possible for a large number of neutrons to be evaporated. The mean values and dispersion of the neutron multiplicity distribution predicted by the cascade–evaporate–fission–multifragmentation model are presented in Figs. 3c and 3d. The values calculated are in good agreement with those obtained in the experiments with real photons absorbed by a lead nucleus [48].

It should be noted that Fig. 3 shows only mean values of the excitation energy, whereas a small fraction of absorbed hard photons can lead to considerable heating of the nucleus caused by a multipion system passing through. This phenomenon was studied in some detail in [30], where it was shown that the part of events with high excitation energy, which leads to a multifragmentation of residual nuclei, can be large enough, up to 10–15% of the total cross section of electromagnetic dissociation.

Another clear manifestation of the impact produced by a multipion system on a heavy nucleus that has absorbed a photon is the formation of a broad ensemble of residual nuclei produced upon knocking a large number of nucleons out of the target nucleus.[4] In [39] such processes were studied by absorbing the photons with energies up to 4 GeV by easily fissionable nuclei (Th, U, and Np). With the RELDIS model it was shown that the majority of produced residual nuclei have an appreciably lower fission probability. Indeed, as a result of losing a large number of nucleons by the target nucleus, residual nuclei significantly differ from the initial easily fissionable nucleus. Therefore, contrary to expectations, growth in the photon energy does not increase the fission probability of the target nucleus.

[4] The term "photospallation reactions" is frequently used.

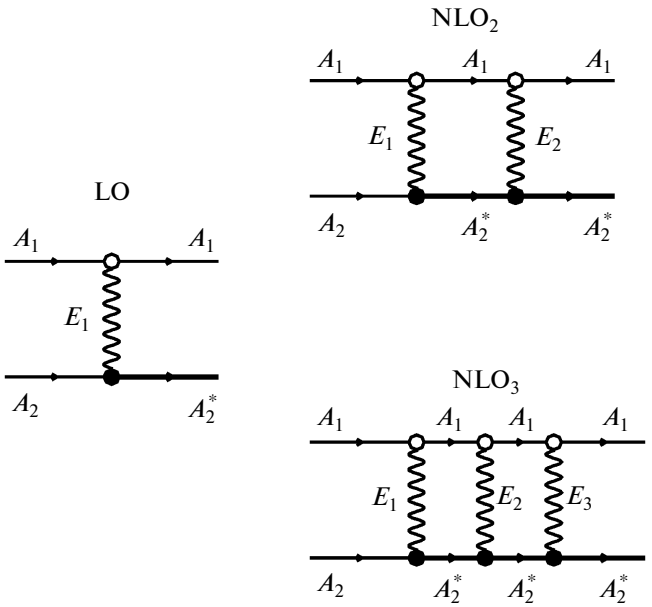

Fig. 4. Single dissociation of nuclei in leading order (LO) and next-to-leading order with exchange by two (NLO_2) and three (NLO_3) photons. Photon emission with no change in the nuclear state is denoted by the light vertex, and photon absorption with nuclear excitation or particle production by the dark one.

3. SINGLE ELECTROMAGNETIC DISSOCIATION OF PROJECTILE NUCLEI

It was shown in the previous section how the spectrum of equivalent photons is calculated within the RELDIS model and how the interaction of such photons with nuclei is simulated. Various processes of low- and high-energy photon absorption by nuclei were presented. Now let us consider directly the electromagnetic dissociation of relativistic and ultrarelativistic nuclei.

Let us consider ultraperipheral collisions of nuclei with mass numbers and charges (A_1, Z_1) and (A_2, Z_2) that have radii R_1 and R_2, respectively. Among the processes shown in Fig. 4, the nucleus A_1 emits one or several photons but stays in its ground state. On the contrary, photoabsorption by the nucleus A_2 leads to its transition to the excited state A_2^* and, as a rule, to nuclear disintegration. Such a process is called electromagnetic dissociation of the A_2 nucleus.

The average number of photons absorbed by the A_2 nucleus during collisions with the impact parameter b is calculated in [49] as follows

$$m_{A_2}(b) = \int_{E_{\min}}^{E_{\max}} N_{Z_1}(E_1, b)\sigma_{A_2}(E_1)dE_1. \qquad (12)$$

Here the spectrum of equivalent photons from Eq. (4) is used, along with the corresponding total cross sec-

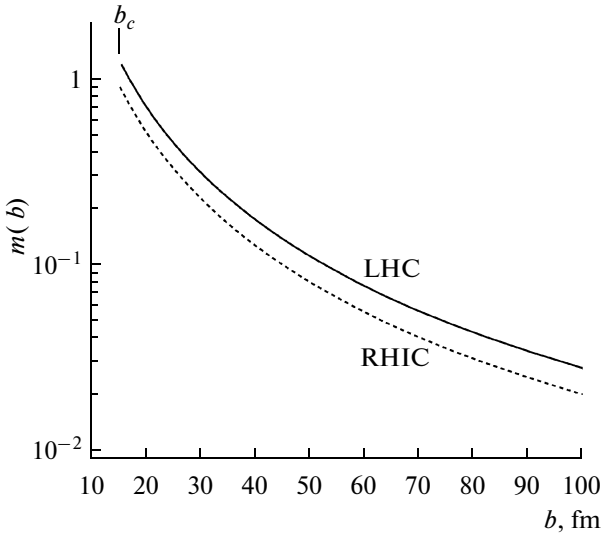

Fig. 5. Mean numbers of equivalent photons absorbed in ultraperipheral collisions of nuclei as a function of the impact parameter [14]. The values for AuAu collisions at beam energies of 100A + 100A GeV (dashed curve) and PbPb collisions at 2.75 A + 2.75 A TeV (solid curve) are presented for the RHIC and LHC colliders, respectively.

tion $\sigma_{A_2}(E_1)$ of photoabsorption with a given energy on the A_2 nucleus measured in the photonuclear experiments [50–53] or predicted by theory [54].

For the collisions of gold and lead nuclei we are interested in, we shall use experimental data on the total photoabsorption cross sections from [43, 45, 55, 56]. In the vicinity of GR, let us use a set of approximations in the form of the Lorentzian curves taken from review [50]. Guided by the advice given in [56], the total photoabsorption cross sections measured in [43, 55] for Au and Pb nuclei should be multiplied by 0.93 and 1.22, respectively. In the region of the quasideuteron photoabsorption, Eq. (11) provides a good approximation for the total cross section.

Above the pion production threshold, at $E_\gamma \geq 140$ MeV the total photoabsorption cross section is proportional to the number of nucleons in a target nucleus: $\sigma_A(E_\gamma) \propto A$. Such a universal dependence follows, in particular, from the results of recent measurements [52, 53]. Thus, the cross section per bound nucleon, $\sigma_A(E_\gamma)/A$, has almost the same value for light, medium, and heavy nuclei, for example, C, Al, Cu, Sn, or Pb, at least up to $E_\gamma \sim 3$ GeV. Therefore, the experimental data obtained for just one nucleus allow the cross sections for other nuclei to be calculated. However, it should be noted that, in this energy range, the universal curve $\sigma_A(E_\gamma)$ appreciably differs from the extrapolation of the cross sections on free nucleons: $(Z\sigma_{\gamma p} + N\sigma_{\gamma n})/A$ [53].

For $E_\gamma > 3$ GeV, deviation from the universal dependence is observed. For example, $\sigma_A(E_\gamma)/A$ for lead proves to be 20–25% lower than that for carbon [54, 57] because of the nuclear shadowing effect. To calculate $\sigma_A(E_\gamma)$ for $E_\gamma > 3$ GeV, the Glauber–Gribov scattering theory has been used, along with the generalized vector dominance model [54, 57]. Such an approach successfully describes in general the data on absorption of high-energy photons by nuclei. It should be noted that these data suffer large uncertainties in the region $E_\gamma > 10$ GeV.

The lower integration limit $E_{\min}$ in Eq. (12) corresponds to the lowest energy of an equivalent photon that still allows a nucleus to disintegrate. For heavy nuclei this is the threshold of a neutron photoemission reaction, which is approximately 7 MeV. The upper limit of integration is determined by the quantity $E_{\max} \approx \gamma/(R_1 + R_2)$; see Subsection 2.1. Following [15, 49] we assume that the probability of a multiple photon absorption is controlled by the Poisson distribution with the mean number of absorbed photons $m_{A_2}(b)$ defined by Eq. (12). The values of $m(b)$ are displayed in Fig. 5 for ultraperipheral collisions of gold and lead nuclei at the RHIC and LHC colliders, respectively.

3.1. Leading Order Single Electromagnetic Dissociation of Nuclei

We consider a single electromagnetic dissociation of the A_2 nucleus taking place into a certain decay channel i. The leading order of this interaction is represented by the diagram LO in Fig. 4 and corresponds to the one-photon exchange. The term "single electromagnetic dissociation" is meant to label those ultraperipheral interactions where a disintegration of one nucleus is registered. This concept is not related with the number of photons exchanged between colliding nuclei. It will be shown below that a single electromagnetic dissociation can occur as a result of absorbing two or three photons.

Following [49] we write down the probability for absorbing a single photon with arbitrary energy in a collision with the impact parameter b,

$$P_S(b) = m_{A_2}(b)e^{-m_{A_2}(b)}, \qquad (13)$$

and the probability density for absorbing a single photon with certain energy E_1, again, in a collision with the impact parameter b as follows:

$$q_S(E_1, b) = \frac{N_{Z_1}(E_1, b)\sigma_{A_2}(E_1)}{m_{A_2}(b)}. \qquad (14)$$

Using the branching ratio $f_{A_2}(E_1, i)$ of the i channel, defined as the relative probability of the A_2 nucleus decaying into this channel caused by absorption of a photon with energy E_1, we write the partial dissocia-

tion cross section $d\sigma^{\mathrm{SED}}_{A_2}(i)/dE_1$[5] for the i channel in the LO process with a photon having energy E_1:

$$\frac{d\sigma^{\mathrm{SED}}_{A_2}(i)}{dE_1} = 2\pi\int_{b_c}^{\infty} dbbP_S(b)q_S(E_1, b)f_{A_2}(E_1, i). \quad (15)$$

The quantities $f_{A_2}(E_1, i)$ will be computed by using the Monte Carlo method in combination with the cascade model of photonuclear reactions combined with the models of evaporation, fission, and multifragmentation of residual nuclei mentioned in Section 2.2. Selection of a minimal impact parameter b_c, which separates the regions of nuclear and electromagnetic interactions, will be discussed later on.

To calculate the cross section of electromagnetic dissociation (LO) with the A_2 nucleus disintegrating into the i channel it is necessary to integrate the expression in (15) over the equivalent photon energy,

$$\sigma^{\mathrm{SED}}_{A_2}(i) = \int_{E_{\min}}^{E_{\max}} dE_1 N^{\mathrm{SED}}_{Z_1}(E_1)\sigma_{A_2}(E_1)f_{A_2}(E_1, i), \quad (16)$$

by first defining the spectral function for electromagnetic dissociation with the one-photon exchange:

$$N^{\mathrm{SED}}_{Z_1}(E_1) = 2\pi\int_{b_{\min}}^{\infty} dbbe^{-m_{A_2}(b)}N_{Z_1}(E_1, b). \quad (17)$$

Note that such a definition is convenient in that it lets the expressions to be found in Eqs. (12) and (17) be calculated by means of the standard numerical integration methods and, then, save results as tables for their subsequent interpolation. Because of the long-range nature of electromagnetic interactions, evaluation of the integral in (17) requires a special approach. A sufficient accuracy of calculations can be achieved by splitting the integration interval into two subintervals: $[b_{\min}, b_{\mathrm{cut}}]$ and $[b_{\mathrm{cut}}, \infty)$. The quantity b_{cut} is fixed by the condition $e^{-m(b_{\mathrm{cut}})} \approx 1$, which allows us to neglect the exponential factor in the second interval. Thereafter, the first term in (17) is found by numerical integration, while the second is analytically calculated, giving the familiar expression [33]. The subsequent integration in (16) is carried out using the Monte Carlo method and gives a partial cross section of electromagnetic dissociation into the i channel.

The total cross section of electromagnetic dissociation is computed by employing (16) with the branching ratio of a certain channel replaced by an overall probability of all channels which is unity by definition: $f_{A_2}(E_1, i) \longrightarrow 1$. Thus, a product of the spectrum of equivalent photons and the total photonuclear cross section defines the total cross section. This product is displayed in Fig. 6 as a function of the equivalent photon energy. The cases of electromagnetic dissociation of gold and lead nuclei shown in Fig. 6 will be considered below.

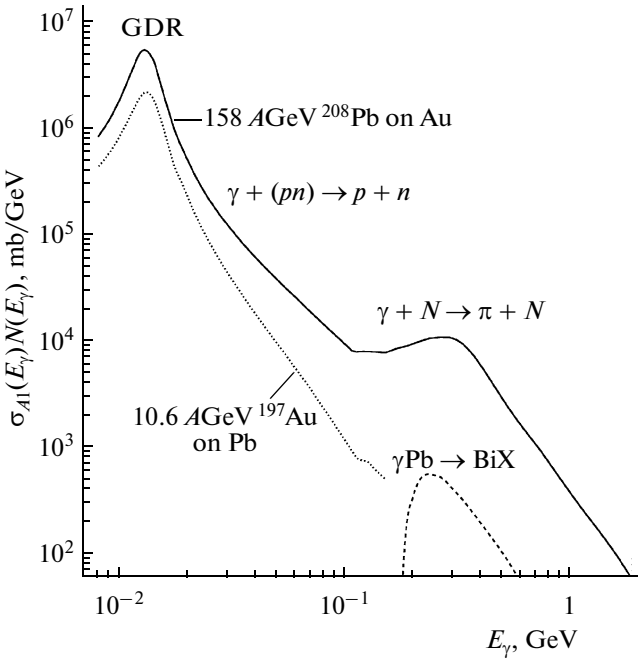

Fig. 6. Product of the spectrum of equivalent photons and total photonuclear cross section for 10.6 A GeV gold nuclei (dotted curve) and 158 A GeV lead nuclei (solid curve) in the interactions with gold and lead targets, respectively. The regions of GR excitation, quasi-deuteron absorption, and Δ-isobar excitation are shown. For comparison, a product of the photon spectrum at an energy of 158 A GeV and the partial cross sections of photonuclear reactions with $_{83}$Bi (dashed curve) is shown.

In what follows it will be convenient to rewrite Eq. (16) by changing the order of integration:

$$\sigma^{\mathrm{SED}}_{A_2}(i) = 2\pi\int_{b_c}^{\infty} dbbP_{A_2}(b, i). \quad (18)$$

Here the probability of A_2 dissociating into the i channel for a given impact parameter b is defined as follows:

$$P_{A_2}(b, i) = e^{-m_{A_2}(b)}\int_{E_{\min}}^{E_{\max}} dE_1 N_{Z_1}(E_1, b) \times \sigma_{A_2}(E_1)f_{A_2}(E_1, i). \quad (19)$$

3.2. Next Order Processes of Electromagnetic Dissociation

As is shown in Fig. 5, the average number of virtual photons $m(b)$ absorbed in the collisions with a given impact parameter b can be close to unity at small b. In

[5] SED stands for single electromagnetic dissociation.

this case a Poisson distribution for the number of absorbed photons yields an appreciable probability of the processes with two or three exchanged photons, which are denoted in Fig. 4 via NLO_2 and NLO_3, respectively.

We write the probability of absorbing exactly two photons by the A_2 nucleus in a collision with an impact parameter b:

$$P_D(b) = \frac{m_{A_2}^2(b)}{2!}e^{-m_{A_2}(b)}. \quad (20)$$

Accordingly, the probability density of the above reaction in which two photons have energies E_1 and E_2 is defined as follows:

$$q_D(E_1, E_2, b) = \frac{N_{Z_1}(E_1, b)\sigma_{A_2}(E_1)N_{Z_1}(E_2, b)\sigma_{A_2}(E_2)}{m_{A_2}^2(b)}. \quad (21)$$

This allows the partial cross section $d^2\sigma^{DED}/dE_1dE_2$[6] of A_2 nucleus dissociation into i channel to be written as a result of the NLO_2 process with exchange of two photons with energies E_1 and E_2:

$$\frac{d^2\sigma_{A_2}^{DED}(i)}{dE_1dE_2} = 2\pi\int_{b_{min}}^{\infty} dbbP_D(b)q_D(E_1, E_2, b) \times f_{A_2}(E_1, E_2, i). \quad (22)$$

Here the branching ratio $f_{A_2}(E_1, E_2, i)$ of the i channel denotes the probability for the A_2 nucleus to decay into this channel resulting from absorption of two photons. The quantity $f_{A_2}(E_1, E_2, i)$ is also calculated by using the cascade–evaporation–fission–multifragmentation model presented in Subsection 2.2. To this end, the Monte Carlo method is used to simulate absorption of two photons in each photoabsorption event.

Integrating the quantities E_1 and E_2 out yields the cross section of NLO_2 process with the A_2 decay into the i channel:

$$\sigma_{A_2}^{DED}(i) = \int_{E_{min}}^{E_{max}}\int_{E_{min}}^{E_{max}} dE_1dE_2\mathcal{N}_{Z_1}^{DED}(E_1, E_2) \times \sigma_{A_2}(E_1)\sigma_{A_2}(E_2)f_{A_2}(E_1, E_2, i), \quad (23)$$

where the spectral function is defined as follows:

$$\mathcal{N}_{Z_1}^{DED}(E_1, E_2) = \pi\int_{b_c}^{\infty} dbbe^{-m_{A_2}(b)} \times N_{Z_1}(E_1, b)N_{Z_1}(E_2, b). \quad (24)$$

[6] DED stands for double-photon electromagnetic dissociation.

By analogy with the calculation of (17), the integration region in Eq. (24) can be split by the quantity b_{cut} into two intervals. For $b > b_{cut}$ and, hence, for $\times \gg 1$ the following asymptotic relation is used:

$$K_1(\times) \approx \sqrt{\pi/2\times}e^{-\times}, \quad (25)$$

which upon integration gives a special function referred to as the exponential integral. The methods of calculating (17) and (24) described above enable us to provide sufficient accuracy for results at a relatively large integration step within a wide range of the impact parameter b.

The process with three photons shown in Fig. 4 is denoted as NLO_3. Expressions analogous to $\sigma_{A_2}^{DED}(i)$ can also be obtained for the decay probability into the i channel in the processes with three and even four photons. Here we cite only the total cross section of a single electromagnetic dissociation with the exchange of at least three photons, corresponding to the processes NLO_{3+}, which is written as a sum of the terms $[m_{A_2}^n(b)/n!]$ for $n \geq 3$ (see [14]):

$$\sigma_{A_2}^{TED} = 2\pi\int_{b_c}^{\infty} dbbe^{-m_{A_2}(b)}\sum_{n=3}^{\infty}\frac{m_{A_2}^n(b)}{n!}. \quad (26)$$

Since the probability of nuclear collision without a photon exchange is $\exp[-m_A(b)]$, the sum of contributions coming from all the photon exchange processes was written in [58] as follows:

$$\sigma_{tot}^{SED} = 2\pi\int_{b_c}^{\infty} dbb[1 - e^{-m_A(b)}]. \quad (27)$$

To simulate one- or two-photon exchange processes, the dedicated computer code RELDIS that uses the Monte Carlo method has been developed. The calculation starts with tabulating the values of spectral functions (17) and (24). Thereafter, the total cross sections of electromagnetic dissociation σ^{SED} and σ^{DED} are computed. The relation between these quantities defines fractions of events with a one- or two-photon absorption to be generated during subsequent simulation of the fragmentation by means of the Monte Carlo procedure. The cascade–evaporation–fission–multifragmentation model is used to simulate a given number of events with interactions of equivalent photons with a nucleus. The photon energies in one- or two-photon events are randomly generated weighted by spectral functions (17) and (24), respectively. The calculations are done in the rest frame of a nucleus, which absorbs a photon, with subsequent Lorentz transformation of four-momenta of the produced particles to the laboratory frame. Once a necessary number of events are generated and required histograms are filled in, the latter are multiplied by σ^{SED} and σ^{DED} so as to find absolute values of the cross sec-

Table 2. Total cross sections (in units of barns) of electromagnetic dissociation in AuAu and PbPb collisions at the RHIC and LHC colliders calculated by using the RELDIS model [32] and in [11, 28, 58]. The cross sections of LO and LO_2 processes are given along with their sum. For comparison, the total cross sections of hadronic interactions of nuclei computed by using the abrasion–ablation model are presented

	Type of fragmentation	σ^{SED}(LO)	σ^{DED}(NLO_2)	Sum
65 + 65 *A* GeV AuAu	Single electromagnetic dissociation	82	1.78	83.8
	Hadronic interaction	–	–	7.29
100 + 100 *A* GeV AuAu	Single electromagnetic dissociation	93.2	1.86	95.1
				88 [11]
				95 [28]
	Hadronic interaction			7.29
				7.09 [58]
2.75 + 2.75 *A* TeV PbPb	Single electromagnetic dissociation	212	3	215
				214 [11]
				220 [28]
	Hadronic interaction	–	–	7.88

tions of dissociation into certain channels or inclusive cross sections for particle production in the electromagnetic dissociation processes.

The total cross sections for a single electromagnetic dissociation of gold and lead nuclei at the RHIC and LHC colliders are presented in Table 2. Since the density of equivalent photon flux is proportional to Z^2 of a projectile nucleus, large values for σ^{SED} should be expected in the case of ultraperipheral interactions of heavy nuclei. Indeed, the cross sections of electromagnetic dissociation of lead nuclei accelerated at the LHC collider are almost 30 times higher than that of hadronic interactions of nuclei, thus reflecting the long-range nature of electromagnetic interactions.

3.3. Neutron Emission from Gold and Lead Nuclei in Photonuclear Reactions

Accuracy in computing the cross sections for partial channels of electromagnetic dissociation $\sigma_A^{SED, DED}(i)$ is defined, among other factors, by the credibility of the quantities $\sigma_A(E_\gamma)f_A(E_\gamma, i)$, the partial cross sections for different channels of photonuclear reactions, which are part of Eqs. (16) and (23). As is shown in Fig. 6, the GR region yields a leading contribution to $\sigma_A^{SED, DED}(i)$ because of, first, the low-energy part of the equivalent photon spectrum dominating here, and, second, the large values of the cross sections for photonuclear reactions, again, in this particular region. For heavy nuclei the neutron emission is expected to dominate, as the charged particle emission is suppressed by the high Coulomb barrier.

It is possible to estimate uncertainties of the data of photonuclear experiments by comparing the results of independent experiments with each other or confronting experimental data with predictions of widely accepted theoretical models. For many years the photoneutron cross sections for a multitude of target nuclei were measured in Saclay [43, 45, 48] and Livermore [55]. These were then compiled and classified in widely recognized works [50, 51].

For the nuclei we are interested in here, namely, ^{197}Au and ^{208}Pb, the detailed data were primarily obtained for (γ, n) and (γ, $2n$) reactions, whereas the reactions (γ, $3n$) and (γ, $4n$) were less scrutinized (see [43, 55]). The measurements were performed within the energy range $6 \le E_\gamma \le 35$ MeV, where the GR dominates; see Figs. 7 and 8. Since emission of p, d, ^{3}He, and ^{4}He by heavy nuclei is suppressed by the high Coulomb barriers, the sum of partial cross sections for all neutron multiplicities $\sigma(\gamma, n) + \sigma(\gamma, 2n) + \sigma(\gamma, 3n) + \sigma(\gamma, 4n)$ is close to the total photoabsorption cross section. In experiments [43, 45, 48, 55] charged particles were not detected; therefore, each of the measured cross sections $\sigma(\gamma, in)$ with emission of i neutrons is inclusive and includes a small contribution of the channels with emission of charged particles, such as (γ, inp) and (γ, $in\,2p$). Here, the channels (γ, p) and (γ, $2p$) were ignored. As was shown in [45], this led to a small systematic error of ~3–5% in determining the total photoabsorption cross section.

In Saclay [45, 48] the average characteristics of photoabsorption reaction on ^{208}Pb were measured, such as the mean value and width of the neutron multiplicity distribution; see Fig. 3. The data were taken at the energies $35 \le E_\gamma \le 140$ MeV, where the quasi-deuteron mechanism dominates. In addition, the neutron yields $\sum_{i \ge 1} i\sigma(\gamma, in)$ and cross sections for emission of at least j neutrons $\sum_{i \ge j} i\sigma(\gamma, in)$ have been measured.

As far as I know, direct measurements of photoneutron cross sections and multiplicities for the ^{197}Au

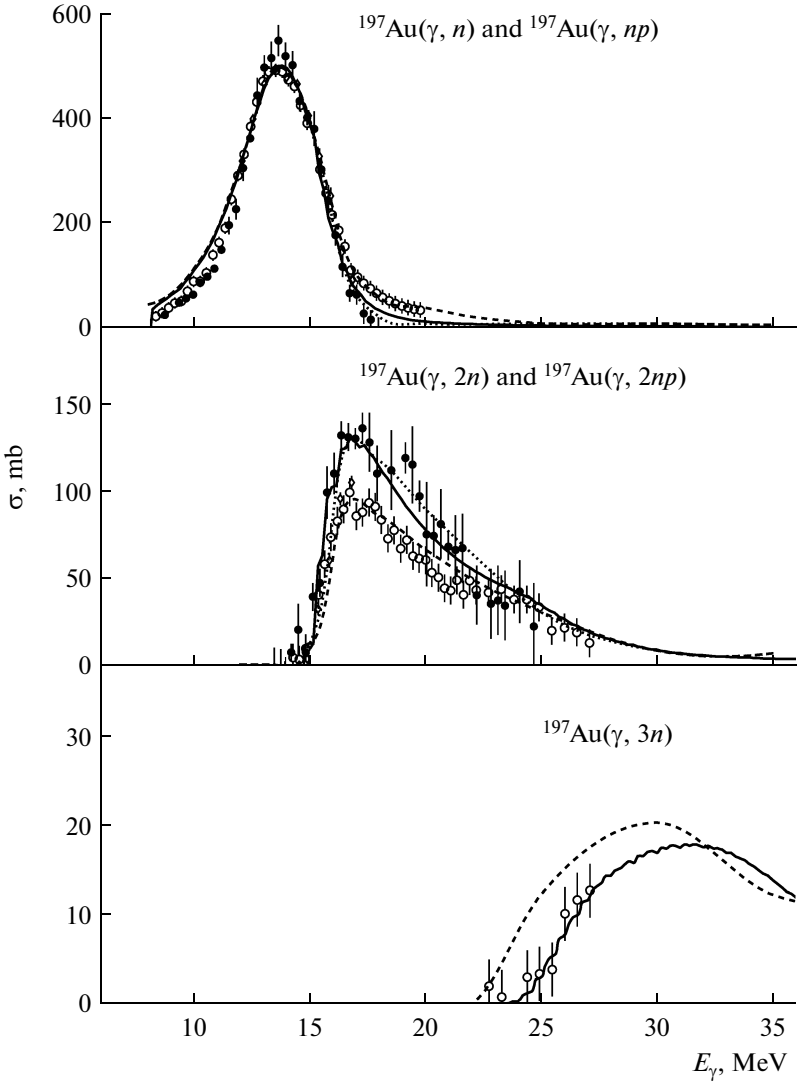

Fig. 7. Photoneutron cross sections for gold nuclei [32]. The light and dark dots denote the Saclay [43] and Livermore [55] data, respectively, corrected according to [56]. The results of the GNASH code are shown by solid curves. The results of the RELDIS code are given by dashed and dotted curves, respectively, for calculation versions that either include or neglect a direct reaction with 1n emission.

nucleus at $E_\gamma > 30$ MeV have not been carried out. The only model-dependent estimate of the mean photoneutron multiplicity has been obtained in [59] from measurements of the mean excitation energy for ^{197}Au at $160 \le E_\gamma \le 250$ MeV.

In general, Figs. 7 and 8 demonstrate good agreement between the data on (γ, n) reaction taken in Saclay and Livermore. Some discrepancy is observed only for the GR peak height (~3% for ^{197}Au and ~20% for ^{208}Pb) and on the right branch of the resonance, where the (γ, n) and (γ, 2n) processes compete with each other. Substantial differences in the cross sections (γ, 2n) measured in various experiments are noticed in both the energy dependence and absolute magnitude. For ^{208}Pb discrepancies are found to reach ~50%.

A few estimates for the photonuclear data were made, along with repeated measurements to eliminate existing discrepancies. It was noted in [60] that the total photoneutron yields σ(γ, n) + 2σ(γ, 2n) + 3σ(γ, 3n) measured in Saclay and Livermore are in good agreement with each other. This observation enabled us to draw the conclusion that the discrepancies in photoneutron cross sections measured in these laboratories are related with the differences in procedures of event selection by the neutron multiplicity which were used in Saclay and Livermore. It was concluded in [60] that the shortcomings of such a procedure used in Saclay caused a fraction of (γ, 2n) events being mistaken for pairs of (γ, n) events.

New measurements conducted in Livermore in 1987 [56] showed that the normalizations of both the

earlier data taken in Livermore [55] and the data taken in Saclay [43] should be modified. In particular, it is recommended to multiply the Saclay results [43] for ^{197}Au and ^{208}Pb by 0.93, which is actually done while using the photonuclear data in the RELDIS. Note that this correction is not generally accepted and, in particular, the authors of [28, 58, 61] use the Saclay data without correcting for their normalization.

New measurements of the (γ, $2n$) reaction cross section were presented in [56] for ^{197}Au and ^{208}Pb. On the one hand, these new results for the (γ, $2n$) reaction and with ^{197}Au turned out to be almost the same as those obtained in Saclay for an identical reaction; therefore, the suggestions of [60] concerning unreliability of the neutron multiplicity sorting procedure slems to be unconfirmed. On the other hand, recent data [56] have been obtained for photon energies merely a few megaelectronvolts above the (γ, $2n$) threshold; therefore, the suggestions made in [60] cannot completely be ruled out.

One of the most recent measurements of (γ, n) cross sections for ^{208}Pb was carried out at Saratov University and presented in [62], where the fine structure of the GR's low-energy part was studied in some detail. The photoneutron cross sections were obtained from the neutron yield curves by using the method of statistical regularization.

The (γ, n) cross section for ^{208}Pb was estimated at Moscow State University [63] by applying the statistical reduction method. Because of systematic errors in calibration and normalization, the integral characteristics of the measured (γ, n) cross sections (an integral over the energy, mean, and other moments of energy dependence) turn out to be different in various experiments [43, 45, 55]. Using the method of statistical reduction, the authors of [63] renormalized both the absolute values of the cross sections and their energy scales. This enabled them to restore agreement between the integral characteristics of (γ, n) cross sections measured in different laboratories.

The data on the (γ, n) reaction with ^{208}Pb nuclei [62, 63] displayed in Fig. 8 are in good agreement with the renormalized Saclay data [43] up to the (γ, $2n$) threshold. Unfortunately, the latter reaction was not studied in [62, 63].

It can now be concluded that the partial cross sections for channels of electromagnetic dissociation of ultrarelativistic nuclei ^{197}Au and ^{208}Pb cannot be calculated by using only photoneutron cross sections measured in the experiments with real photons. Additional information on the photodisintegration of nuclei by equivalent photons within a wide energy range ($E_{\min} \le E_\gamma \le E_{\max}$) can be obtained by employing theoretical models. It is especially crucial for channels with high neutron multiplicity ($\ge$3) and those with charged particles, such as p, d, t, and α, present in addition to neutrons.

It is known that the GNASH model [64] successfully describes neutron emission under irradiation of nuclei by photons [65]. However, since a photoabsorption process is solely modeled by exciting a giant dipole resonance or quasi-deuteron absorption, the region where the model is applicable is bounded from the above by the pion photoproduction threshold: $E_\gamma \le$ 140 MeV.

The total cross section of nuclear photoabsorption in the GNASH model is written as follows [65]:

$$\sigma_A(E_\gamma) = \sigma_{\mathrm{GDR}}(E_\gamma) + \sigma_{\mathrm{QD}}(E_\gamma), \qquad (28)$$

where the GDR cross section σ_{GDR} is fixed by the Lorentzian curves with the parameters from [51] including the corrections from [56]. The cross section of quasi-deuteron absorption σ_{QD} in the GNASH model is calculated similarly to the Levinger model by using the experimental cross section of deuteron photodisintegration σ_d [66]:

$$\sigma_{\mathrm{QD}}(E_\gamma) = L\frac{NZ}{A}\sigma_d(E_\gamma)F(E_\gamma), \qquad (29)$$

where N, Z, and A denote the number of neutrons and protons and the mass number of a nucleus that absorbs a photon. The Levinger parameter is taken to be 6.5. The Pauli exclusion principle applicable to a proton and neutron that absorbed a photon effectively reduces the photoabsorption cross section compared with that on a free deuteron, $\sigma_d(E_\gamma)$. This is taken into account by the factor $F(E_\gamma)$. In [66] $F(E_\gamma)$ was calculated as a multidimensional integral, which in the energy range from 20 to 140 MeV was approximated by the polynomial expression

$$\begin{aligned} F(E_\gamma) = {} & 8.3714\times10^{-2} - 9.8343\times10^{-3}E_\gamma \\ & + 4.1222\times10^{-4}E_\gamma^2 \\ & - 3.4762\times10^{-6}E_\gamma^3 + 9.3537\times10^{-9}E_\gamma^4. \end{aligned} \qquad (30)$$

or the exponent outside this interval

$$F(E_\gamma) = \begin{cases} \exp(-73.3/E_\gamma), & E_\gamma < 20\ \mathrm{MeV} \\ \exp(-24.2/E_\gamma), & E_\gamma > 140\ \mathrm{MeV} \end{cases}.$$

Thus, $F(E_\gamma)$ tends to zero for small E_γ, approaches unity at large E_γ, and also is consistent with the expression given in (30) at 20 and 140 MeV [65]. The deuteron photodisintegration cross section is parameterized as follows:

$$\sigma_d(E_\gamma) = 61.2(E_\gamma - 2.224)^{3/2}/E_\gamma^3, \qquad (31)$$

where E_γ is taken in megaelectronvolts and σ_d is in millibars, as with the previous expressions.

The probability of a nucleus absorbing a photon is calculated by the GNASH model using the expressions for the total cross section (28)–(30), while a preequilibrium nucleon emission itself, as being a result of

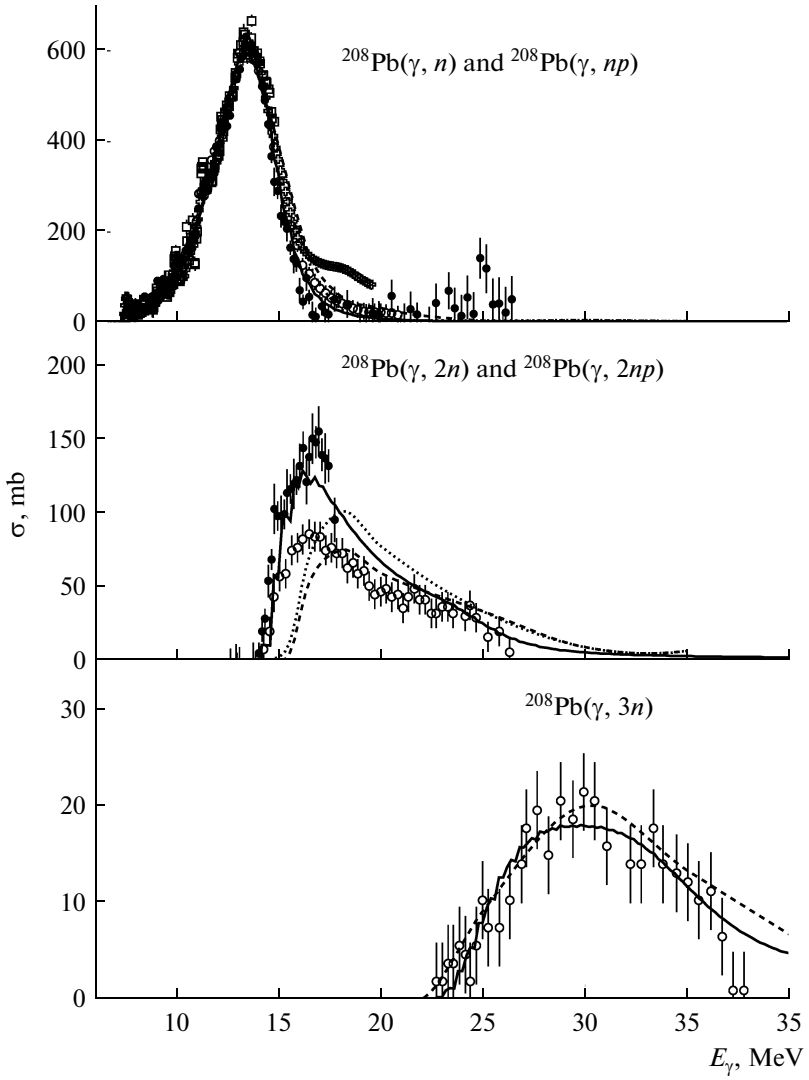

Fig. 8. Photoneutron cross sections for lead nuclei [32]. The light and dark dots denote Saclay [43] and Livermore [55] data, respectively, corrected according to [56]. The crosses represent the data from [62], while the squares show the estimated data from [63]. Remaining notation is identical to that in Fig. 7.

absorption, is described by the exciton model [64, 65]. Following the quasi-deuteron model, a photon is absorbed by a pair of correlated constituent nucleons; therefore, the initial particle–hole configuration is chosen to be $2p1h$ [65] rather than $2p2h$, which would correspond to the absence of correlations between absorbing nucleons. Finally, once equilibrium of a nuclear system is reached, successive particle evaporation is simulated along the lines of the Hauser–Feishbach approach [65].

The results obtained in the framework of the GNASH model for the (γ, n), (γ, 2n), and (γ, 3n) cross sections are also displayed in Figs. 7 and 8 for ^{197}Au and ^{208}Pb nuclei, respectively. The experimental data on (γ, n) and (γ, 3n) reactions are described by the theory reasonably well. Taking into account the discrepancies in the results of different experiments on the (γ, 2n) cross-section measurements, one can note that the GNASH results fall in between the experimental data obtained in Saclay [43] and Livermore [55] for ^{208}Pb. The GNASH results for the (γ, 2n) reaction on ^{197}Au turn out to be rather close to the Livermore data [55]. In general, there is good agreement between the GNASH results and photonuclear experiments [43, 55].

The total cross section $\sigma_A(E_\gamma)$ and branching ratios of the photoabsorption channels $f_A(E_\gamma, i)$ calculated by using the GNASH model can be used to compute the cross sections of electromagnetic dissociation. The restriction $E_\gamma < E_{\max} = 140$ MeV inherent to the model for photonuclear reactions in question has an impact on the result that will be scrutinized in Subsections 5.1 and 5.2.

Note that excitation and subsequent disintegration of a compound nucleus are not the only way to emit neutrons in the process of photon interactions with nuclei in the vicinity of GR. It is known that a GR is described by the theory as a coherent superposition of particle–hole $1p1h$ excitations. A particle or a hole can interact with another nucleon to produce a $2p2h$ excitation. Then, there appear the states $3p3h$, $4p4h$, ..., thus leading to the formation of a system in statistical equilibrium—a compound nucleus. However, contrary to the evolution toward statistical equilibrium, the collective $1p1h$ state can dissociate, emitting a neutron and transiting to the low-lying state of a compound nucleus with an additional hole (see, for example, [67]). As a result of the direct $1n$ emission, the nuclear excitation energy drops to such an extent that the radiation of a second neutron becomes impossible. Therefore, the $(\gamma, 2n)$ reaction in the presence of a direct mechanism turns out to be noticeably suppressed with respect to the purely statistical description of GR.

Although a giant dipole resonance in a ^{208}Pb nucleus dissociates predominantly after reaching statistical equilibrium, the presence of a certain fraction of a direct neutron emission was found in experimental work [68]. In such direct processes, a fast neutron is emitted, while the residual ^{207}Pb nucleus has a total excitation energy less than 3 MeV (see [68]). Another indication of the existence of direct neutron emission in photoabsorption on Au and Pb nuclei was given in [43] based on analysis of competition between $1n$ and $2n$ channels. This confirmed the results of earlier experiments [69, 70], in which the neutron spectrum in photoabsorption processes on the same nuclei was measured. An excess of fast neutrons with kinetic energies ≥4 MeV, as compared with the predictions of the statistic model for GR dissociation, convincingly showed the presence of a direct nucleon emission.

The fraction of the direct processes in ^{208}Pb dissociation with the excitation energy $10 < E^* < 30$ MeV was quantitatively estimated in [67]. It is interesting to note that, outside of this region, the contribution of the direct processes was estimated to be insignificant. Following [43], the portion of the direct mechanisms of a neutron emission in the RELDIS model is estimated to be $P_n^{\mathrm{dir}} = 0.31$ and 0.26 for Au and Pb nuclei, respectively. These numbers are compatible with recent theoretical results presented in [71], where it was shown that the ratio between contributions coming from a direct and statistical neutron emission by a ^{208}Pb nucleus in the GDR region is ~0.1. In the RELDIS model the neutron direct emission angle Θ is randomly generated according to the approximation $W(\Theta) = A + B\sin^2\Theta$ taken from [70]. It is assumed that a direct $1n$ emission takes place at excitation energies $7 \le E^* \le 22$ MeV.

Since the direct emission probabilities P_n^{dir} adopted in the RELDIS model suffer from some uncertainties, the dependence of results on the quantity P_n^{dir} was additionally studied. Part of the calculations were carried out without taking into account direct emission with $P_n^{\mathrm{dir}} = 0$ (see Figs. 7 and 8). As is shown in Fig. 7, the $(\gamma, 2n)$ cross sections on a gold target computed by RELDIS with $P_n^{\mathrm{dir}} = 0.31$ turn out to be reasonably close to the Saclay measurements. However, the Livermore results [55] are best described with $P_n^{\mathrm{dir}} = 0$. Thus, the difference in RELDIS results for partial photoneutron cross sections obtained with $P_n^{\mathrm{dir}} = 0$ and 0.31 approximately matches the level of uncertainty in the data from photonuclear experiments.

3.4. Electromagnetic Dissociation of Nuclei with Neutron Emission

The experimental data on the fragmentation of gold nuclei upon interaction with 158 A GeV ^{208}Pb nuclei [72] confirm that the dominant channel of electromagnetic dissociation of heavy nuclei is neutron emission.

In experiment [72] the processes of one- and two-neutron emission by a ^{197}Au target nucleus were directly studied. The RELDIS results that take into account LO and NLO_2 processes are compared with the experimental data [72] in Table 3. Calculations have been conducted both with and without taking into account direct neutron emission for $P_n^{\mathrm{dir}} = 0.31$ and 0, respectively. The results obtained with $P_n^{\mathrm{dir}} = 0.31$ are in better agreement with experiment; improvement is particularly seen for the $2n$ channel. It is this value of P_n^{dir} that will be used further on. The predictions of the abrasion–ablation model (see Subsection 4.3) are also consistent with experiment.

Neutron emission by 30 A GeV lead nuclei in the collisions with fixed targets was investigated in experiment [73]. The results are displayed in Fig. 9 together with those from RELDIS.

The experimental conditions [73] allowed selection of neutrons with small transverse momenta that were emitted in a forward direction as a result of electromagnetic nuclear excitations, which is confirmed by the typical quadratic dependence of the experimental cross sections of a neutron emission on the charge of a target nucleus Z_T. Indeed, σ/Z_T^2 is nearly independent of Z_T, as it should be expected for electromagnetic processes (lower panel in Fig. 9). Insignificant deviations of the quantity σ/Z_T^2 from a constant value are observed because of the dependence of maximal

Table 3. Partial cross sections of a target nucleus ^{197}Au fragmentation (in *b*) under the impact of lead nuclei with energy 158 *A* GeV [32]. Results of the RELDIS and abrasion models are given. The RELDIS results are shown in parentheses without taking into account direct 1*n* emission. Experimental data are taken from [72]

Dissociation channel	$\sigma^{SED}(i) + \sigma^{DED}(i)$		$\sigma^{nuc}(i)$		All processes	
	Experiment	RELDIS	Experiment	Abrasion	Experiment	Theory
$i = 1n$	26.4 ± 4.0	26.96	0.3 ± 0.1	0.43	26.7 ± 4.0	27.39
$^{197}Au \longrightarrow {}^{196}Au + n$		(25.09)				(25.52)
$i = 2n$	4.6 ± 0.7	4.57	0.13 ± 0.4	0.13	4.7 ± 0.7	4.70
$^{197}Au \longrightarrow {}^{195}Au + 2n$		(6.39)				(6.52)

energy of equivalent photons on the radius of a target nucleus $E_{max} = \gamma/R_T$, which, in its turn, depends on the charge Z_T. For example, in the RELDIS model, $E_{max} = 0.57$ GeV for Pb dissociation on Au, whereas $E_{max} = 0.42$ GeV in PbPb collisions. As is seen from Fig. 9, this leads to a slight (~10%) increase of σ/Z_T^2 for light targets. In general, measured neutron emission cross sections are successfully described by the RELDIS model.

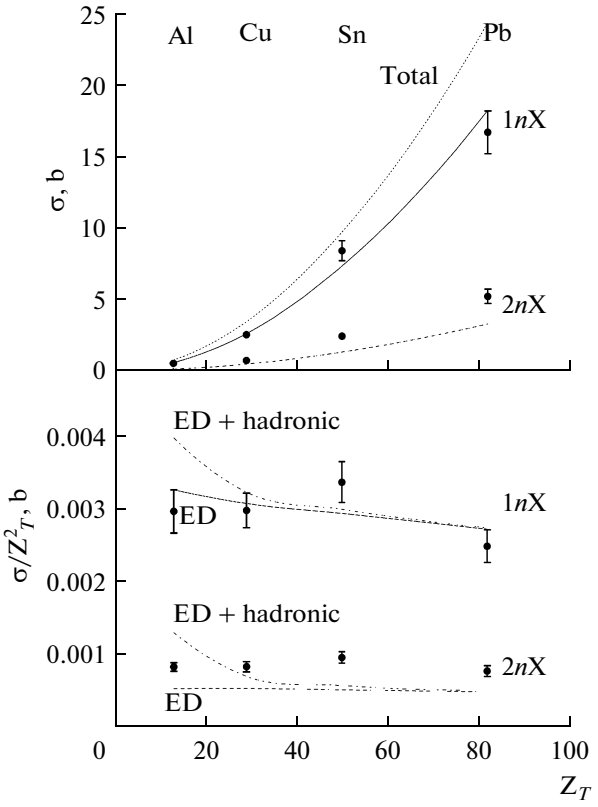

Fig. 9. Upper panel: cross sections of forward emission of one and two neutrons by lead nuclei with energy of 30 *A* GeV produced in interactions with Al, Cu, Sn, and Pb targets (the dots represent measurements from [73]). The RELDIS model results for the total cross section of a single electromagnetic dissociation (dotted curve), 1*n* emission (solid curve), and 2*n* emission (dashed curve) are shown as a function of the target-nucleus charge Z_T. Lower panel: calculated and experimental values of 1*nX* and 2*nX* cross sections after they were divided by Z_T^2. This figure is borrowed from [73].

3.5. Nuclear Interactions Decreasing Nuclear Charge

The cross sections with a change in the charge of ^{208}Pb nuclei with energy of 158 *A* GeV resulting from their single dissociation on lead nuclei, predicted by the RELDIS model, are displayed in Fig. 10 along with the results of measurements taken from [74]. The processes with one (LO) and two (NLO_2) photons shown in Fig. 4 were taken into account in the calculations of electromagnetic dissociation. The cross sections of nuclear fragmentation as a result of the strong interactions were obtained by using the simple abrasion–ablation model. Note that the hadronic nuclear fragmentation occurs via mutual disintegration of nuclei; this is why the abrasion–ablation model will be

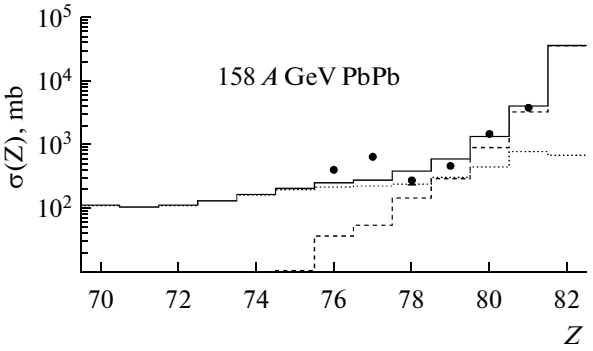

Fig. 10. Partial charge-changing cross sections for ^{208}Pb nuclei with energy 158 *A* GeV on a lead target [32]. The RELDIS model results for electromagnetic dissociation and those of the abrasion–ablation model for fragmentation resulting from the strong interactions are shown by dashed and dotted histograms, respectively. The solid histogram represents their sum, which is compared with experimental data taken from [74] (shown by the full circles).

described in Subsection 4.3 of Section 4, which is devoted to mutual nuclear dissociation.

The loss of protons by a nucleus resulting from the fragmentation is usually accompanied by the process of losing the neutrons as well. The results of calculations for $Z = 82$ correspond to interactions in which a nucleus ^{208}Pb loses neutrons only. Since the experimental setup [74] was not capable of distinguishing secondary nuclei with $Z = 82$ from the beam ones, the cross sections for $Z = 82$ were not measured. As is seen from Fig. 10, the electromagnetic dissociation dominates over the hadronic one for processes with a loss of one, two, and three protons, while the calculated values for these channels are in good agreement with experiment [74].

3.6. Electromagnetic Processes Increasing Nuclear Charge

It was shown in the previous subsection that neutron emission resulting from the electromagnetic interactions can be accompanied by the loss of protons. This leads to the formation of nuclei of other elements with charges less than that of the beam nuclei. Knockout of protons from the nuclei also occurs as a result of hadronic interactions.

On the other hand, nuclear collisions can lead to increasing the charge of one of the colliding nuclei. Because of the strong interactions, a residual nucleus acquires additional protons in several ways. A proton transfer from one partner-nucleus to another is possible at small kinetic energies of colliding nuclei (comparable with the energy of Fermi-motion of constituent nucleons). Quite to the contrary, at relativistic energies of colliding nuclei, the spheres of their Fermi-momenta do not overlap and nucleon transfer from one nucleus to another becomes impossible.

In peripheral collisions of relativistic nuclei, the appearance of additional protons is related with excitation of the Δ resonance and its subsequent decay in nucleon–nucleon collisions: $n \longrightarrow \Delta^0 \longrightarrow p + \pi^-$ [79]. The increase in charge of a residual nucleus results from the proton capture and π^- emission by that nucleus. Such processes may be accompanied by a neutron emission.

In Fig. 11 the charge-pickup cross sections $\sigma(\Delta Z = +1)$ measured in [78, 80, 81] are displayed as a function of the energy of the incident nucleus and the mass of the target nucleus. Within the energy range from 0.5 to 10 A GeV, these cross sections gradually decrease with increasing energy. This is successfully described by the approximation given in [77] that uses the energy dependence of the (p, xn) cross section and depends on the number of protons in a target nucleus Z_T.

Within this energy range, the cross sections $\sigma(\Delta Z = +1)$ depend weakly on the mass number of a target nucleus A_T, which is described by the power-law

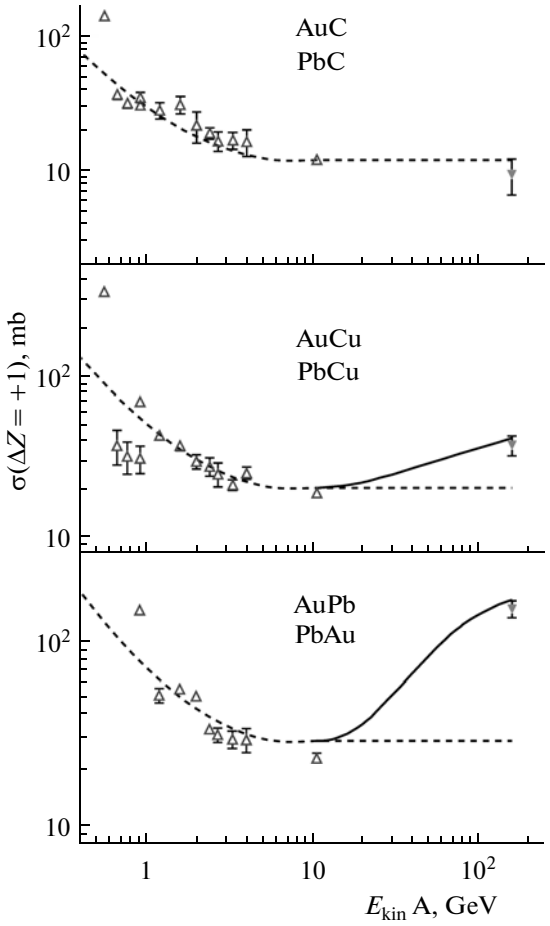

Fig. 11. Energy dependence of the cross sections for charge pickup by Au and Pb nuclei in the collisions with C, Cu, Au, and Pb nuclei [75]. The experimental data from [78, 80, 81] for Au nuclei at energies of up to 10.6 A GeV are shown by open triangles, while those for Pb nuclei at 158 A GeV from [75, 76] are shown by filled ones. Results of approximation from [77] are depicted by dashed curves, while solid ones show the sum of the results obtained by approximation [77] and electromagnetic contribution to the charge pickup processes calculated by using the RELDIS model.

dependence $\sigma(\Delta Z = +1) \propto A_T^{\kappa}$, where $\kappa = 0.223 \pm 0.005$ [81]. In [77] it was assumed that $\sigma(\Delta Z = +1)$ remained constant above ~4 A GeV; therefore, such a behavior of the cross section can be extrapolated up to ~100 A GeV. Such an approximation assumes that the reaction $NN \longrightarrow N\Delta$ is the main process that increases the number of protons in a nucleus, while electromagnetic excitations do not contribute to $\sigma(\Delta Z = +1)$.

However, as the experimental data show [75, 76], bismuth nuclei are produced with an appreciable probability after the passage of 158 A GeV lead nuclei through various targets. The very first explanation of this effect was given in [75, 76]. It was shown that incorporating Δ-isobar excitation on nucleons by virtual photons and, in particular, the photoproduction channel of a negatively charged pion on a neutron

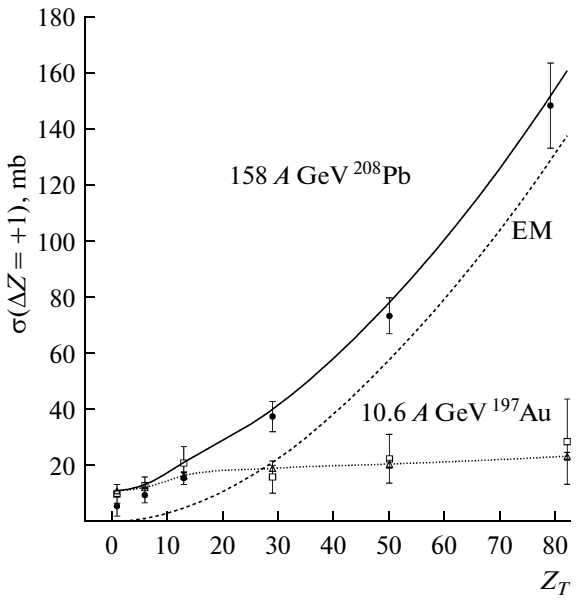

Fig. 12. Cross sections of charge pickup ($\Delta Z = +1$) by gold and lead nuclei as a function of the atomic number Z_T of a target nucleus [76]. The experimental data from [75, 76] for lead nuclei with energies of 158 A GeV are denoted by circles. The solid curve represents the sum of the electromagnetic contribution to $\Delta Z = +1$ cross section (the dashed curve, RELDIS results) and the contribution of the strong interactions (an approximation of experimental data [78, 82] at an energy of 10.6 A GeV, the dotted curve). The data from [78, 82] are shown by triangles and squares, respectively.

$\gamma n \longrightarrow \pi^- p$ into the RELDIS model makes it possible to successfully describe the measured cross section $\sigma(\Delta Z = +1)$. The formation of bismuth nuclei is caused by the subsequent proton capture and π^- emission by a residual nucleus.

Indeed, the contribution of electromagnetic processes to the charge-changing cross section is extremely small for ions with lower energies ($\gamma \le 10$), since the maximal energy of equivalent photons does not exceed the threshold of pion photoproduction. In contrast, at ion energy of 158 A GeV, a considerable portion of the spectrum of equivalent photons exceeds this threshold. As is shown in Fig. 6, photoexcitation of giant resonances and quasi-deuteron absorption of photons dominate at all energies, but Δ resonance excitation becomes important at 158 A GeV.

As is seen from Fig. 11, the RELDIS results successfully describe the experimental data [75, 76] and prove the necessity of taking into account the contribution coming from electromagnetic excitations to the cross section $\sigma(\Delta Z = +1)$ at higher energies. The cross section $\sigma(\Delta Z = +1)$ decreases until the energy reaches 10 A GeV, but then starts to increase because of channels $\gamma N \longrightarrow \pi N$ coming into play. Such an effect can only be neglected in interactions of lead nuclei with the lightest targets, for example, a carbon one, where the contribution of electromagnetic processes is small. This is why their contribution (~1 mb) to $\sigma(\Delta Z = +1)$ depicted in the upper panel in Fig. 11 is almost indiscernible.

The cross sections of a charge pickup by gold and lead nuclei, which were measured in [78, 82] and [75, 76], respectively, are displayed in Fig. 12 as a function of the atomic number Z_T of a target nucleus. The contributions of electromagnetic and strong interactions were not distinguished in the experiments. Following [77] we assume that the contribution coming from the strong interactions depends weakly on the energy for $\gamma \ge 10$; thus, it is almost the same for lead and gold nuclei at 158 A GeV. This contribution can be estimated by using the data taken from [78], where experimental results for 10.6 A GeV gold ions are obtained with small statistical errors. In order to compare predictions of the RELDIS model with the experimental data [75, 76] we add the data from [78] to the theoretical values. Figure 12 demonstrates very good agreement between the final curve and experimental cross sections $\sigma(\Delta Z = +1)$ from [75, 76].

In conclusion, we note that the processes of proton production resulting from charge exchange (excitation of Δ-isobar by exchanging π and ρ mesons) described above and considered in [83] do not explain the experimental results presented in [75, 76]. The charge-changing cross section mechanism is possible only in peripheral nuclear interactions for which the cross section is just a small part of the total one, since it corresponds to the area of a thin ring with a radius close to the impact parameter b_c that separates the regions of electromagnetic and strong interactions (see Subsection 3.1). Therefore, a calculated value for the cross section close to the experimental one can only be obtained (see [83]) by assuming that an excessively large number of nucleons take part in peripheral nuclear interactions, which is not correct. Only resorting to the RELDIS model allows one to explain the experimental results [75, 76].

4. MUTUAL ELECTROMAGNETIC AND HADRONIC DISSOCIATION OF COLLIDING NUCLEAR BEAMS

In Section 3 we have studied ultraperipheral nuclear interactions, in which electromagnetic dissociation of only one partner-nucleus—either a projectile or a target nucleus—is registered in each event. The experiments mentioned above allowed detecting dissociation of either a projectile or target nucleus. In each such collision, a partner-nucleus serves as a source of electromagnetic field that breaks up another nucleus. Note that at the same time it can itself undergo fragmentation in the same collision because of an impact on it from the field of another nucleus. As will be shown below, events with nuclei mutually dissociated by their Coulomb fields are of special interest. Such processes will be called mutual electromagnetic

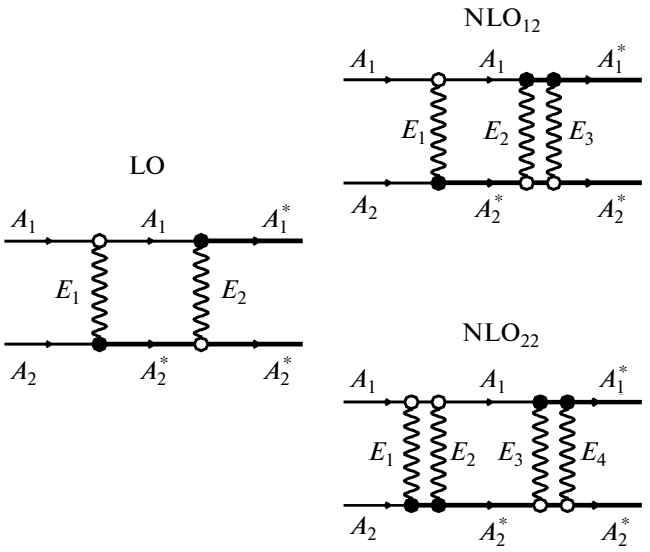

Fig. 13. Mutual dissociation of nuclei in the leading (LO) and next-to-leading orders with exchange by three (NLO_{12}) and four (NLO_{22}) photons. Photon emission without changing the nuclear state is denoted by the light vertex, while photon absorption with nuclear excitation or particle production is shown by the dark one.

dissociation (MED). The processes of mutual electromagnetic dissociation of ultrarelativistic nuclei were thoroughly considered in [32], where the RELDIS model was developed to calculate events of mutual electromagnetic dissociation using the Monte Carlo procedure. Later, other authors in [84] studied the processes of mutual photon absorption that lead to the production of ρ mesons accompanied by nuclear dissociation.

The theory of the processes of mutual electromagnetic dissociation of nuclei will be given along the lines to be found in [14, 32]. The processes of mutual nuclear excitation and their dissociation resulting from two-, three-, and four-photon exchange are displayed in Fig. 13.

Note that mutual electromagnetic dissociation is possible with just one-photon exchange (see Fig. 14). Indeed, photon emission may be accompanied by nuclear excitation, say, GR excitation. To describe such an inelastic process, it is necessary to consider a nucleus-emitter as a quantum object that can transit from the ground to excited states; see [85–87]. As is shown in [85, 86] (see also the discussion in [12]), the cross section of mutual excitation of heavy partner-nuclei by exchanging just one photon (Fig. 14) turns out to be considerably lower than that with two-photon exchange (LO in Fig. 13). The reason behind this is, in the first place, the incoherent photon emission, since the cross section for this inelastic process is proportional to Z of a nucleus-emitter (as opposed to the coherent process without changing a nuclear state for which the cross section is proportional to Z^2) [85].

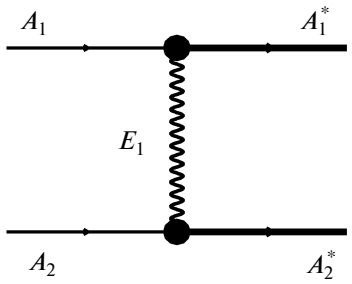

Fig. 14. Mutual dissociation of nuclei with one-photon exchange. Vertices denote photon emission with nuclear excitation, as well as photon absorption that results either in nuclear excitation or in particle production.

Second, upon integrating the momentum, transfer out of the inelastic nuclear form factor makes a substantially lower contribution than the elastic one [86].

For example, for AuAu and PbPb collisions, the cross sections of mutual giant dipole resonance excitation resulting from one-photon exchange depend weakly on the energy and are found to be 0.49 and 0.54 mb, respectively [85]. In [12] the A dependence of such a cross section is defined as $10^{-5} A^2$ mb, which yields 0.39 and 0.43 mb for the nuclei under discussion. As will be shown in the next subsections, the cross sections of processes of mutual electromagnetic dissociation in AuAu and PbPb collisions with exchange by two or more photons (LO, NLO_{12}, and NLO_{22}, Fig. 13) have values of the order of a few millibars and significantly exceed that of the one-photon process of mutual dissociation. Therefore, only coherent processes of photon emission with no change to a nucleus-emitter's state will be considered in what follows.

Let us consider collisions of the identical nuclei ($A_1 = A_2 = A$, $Z_1 = Z_2 = Z$, and $R_1 = R_2 = R$) that are most often studied at nucleus–nucleus colliders. The result of collisions is nuclear fragmentation and production of elementary particles. In experiments at colliders, detection of the direction of nuclear fragment emission allows one to identify the beam in which the nuclear fragmentation took place. Therefore, despite the identity of the masses and charges of colliding nuclei, indices 1 and 2 allow distinguishing which one of the partners underwent fragmentation. The expressions obtained can be generalized to the case of asymmetric collisions.

4.1. Leading Order Mutual Electromagnetic Dissociation

The light and dark vertices in Fig. 13 represent elastic and inelastic processes, respectively. For example, in the leading order process (LO in Fig. 13), the A_1 and A_2 nuclei exchange photons with energy E_1, with the A_2 nucleus transiting to an excited state A_2^* after absorb-

ing such a photon. During the same process, the A_2^* and A_1 nuclei exchange photons with energy E_2, with the A_1 nucleus transiting to the excited state A_1^* upon absorbing a photon. All these lead to excitation and subsequent dissociation of both nuclei.

The diagram NLO_{12} is obtained from LO by adding a third photon E_3 bringing an additional excitation energy to the A_1 nucleus. Note that, in addition to the diagram NLO_{12}, there is an NLO_{21} diagram in which the A_2 nucleus is excited by absorbing two photons and the A_1 nucleus by just by a single photon.

The sequence in which the photons E_1, E_2, E_3, and E_4 are exchanged is not important for computing the cross sections of electromagnetic dissociation; therefore, time ordering is henceforth neglected. Indeed, since the equivalent photon energy is restricted $E_1 \le E_{\max}$ ($E_{\max}$ is given by (9)), its emission cannot alter in a significant way the energy of a relativistic nucleus with mass M_A that emits a photon $E_A = \gamma M_A$. To prove this let us calculate the ratio

$$r = \frac{E_{\max}}{E_A} \approx \frac{1}{RM_A}, \tag{32}$$

that is close to 10^{-4} for heavy nuclei. For such nuclei both the energy and momentum of a nucleus-emitter remain almost unaltered after emitting the first and all subsequent photons. In other words, the first and all subsequent photon exchanges can be considered as processes independent of each other and taking place during the short time span in which the Coulomb fields of nuclei overlap.

To simplify calculations let us assume that the spectra of equivalent photons emitted by a nucleus in its ground and excited states are the same. This is justified by the short duration of the nuclear collision, which turns out to be much shorter than the time, which takes a nucleus to become deexcited and during which, for example, nucleons evaporate or fission occurs. Interference between the processes displayed in Fig. 13 is also neglected, thus rendering their examinations independent of each other.

The expression in (18) can be generalized to the case of mutual dissociation. For instance, the cross section of the LO process leading to dissociation of A_1 and A_2 nuclei into the i and j channels is found to be

$$\sigma_{\mathrm{LO}}^{\mathrm{MED}}(i|j) = 2\pi \int_{b_c}^{\infty} dbb P_{A_1}(b,i) P_{A_2}(b,j), \tag{33}$$

where $P_{A_1}(b,i)$ and $P_{A_2}(b,j)$ are defined by the expression quoted in (19) to be the probabilities for A_1 and A_2 nuclei to dissociate into the i and j channels, respectively. The lower limit of integration b_c separates the regions of hadronic and electromagnetic interactions of nuclei. Similarly to the expression in (18) it approximately is equal to the sum of radii of nuclei $b_c \approx R_{A_1} + R_{A_2}$. Selecting b_c will further be discussed in Subsection 4.3.

The total cross section of LO process is obtained by replacing the branching ratio of a certain channel in (19) by their overall sum, which is unity by definition, $f_{A_1}(E,i) \longrightarrow 1$ and $f_{A_2}(E,j) \longrightarrow 1$:

$$\begin{aligned}\sigma_{\mathrm{LO}}^{\mathrm{MED}} &= 2\pi \int_{b_c}^{\infty} dbb [m_{A_1}(b) e^{-m_{A_1}(b)}][m_{A_2}(b) e^{-m_{A_2}(b)}] \\ &= 2\pi \int_{b_c}^{\infty} dbb m_A^2(b) e^{-2m_A(b)}.\end{aligned} \tag{34}$$

It is assumed that $A_1 = A_2$ in the latter equality.

4.2. Next Order Processes of Mutual Electromagnetic Dissociations

In addition to the LO process of electromagnetic dissociation, we now consider next-to-leading (NLO) ones with three or four photons exchanged. The total cross section of the NLO_{12} three-photon exchange depicted in Fig. 13 is written as follows:

$$\begin{aligned}\sigma_{\mathrm{NLO}_{12}}^{\mathrm{MED}} &= 2\pi \int_{b_c}^{\infty} dbb [m_{A_1}(b) e^{-m_{A_1}(b)}]\left[\frac{m_{A_2}^2(b)}{2} e^{-m_{A_2}(b)}\right] \\ &= 2\pi \int_{b_c}^{\infty} dbb \frac{m_A^3(b)}{2} e^{-2m_A(b)},\end{aligned} \tag{35}$$

where the last equality is derived under the condition $A_1 = A_2$. The process NLO_{21}, which proceeds via excitation of A_2 nucleus by absorbing two photons, has the same cross section.

The cross section of the process with the NLO_{22} four-photon exchange displayed in Fig. 13 takes the following form:

$$\begin{aligned}\sigma_{\mathrm{NLO}_{22}}^{\mathrm{MED}} &= 2\pi \int_{b_c}^{\infty} dbb \left[\frac{m_{A_1}^2(b)}{2} e^{-m_{A_1}(b)}\right]\left[\frac{m_{A_2}^2(b)}{2} e^{-m_{A_2}(b)}\right] \\ &= 2\pi \int_{b_c}^{\infty} dbb \frac{m_A^4(b)}{4} e^{-2m_A(b)},\end{aligned} \tag{36}$$

where the last equality is once again derived under the condition $A_1 = A_2$.

Processes in which at least one of the colliding nuclei absorbs three photons are given in Fig. 15. A set of such processes with exchange of four (NLO_{13}), five (NLO_{23}), and six (NLO_{33}) photons (including diagrams with permutation of A_1 and A_2 nuclei) will be denoted as $\mathrm{NLO}_{\mathrm{TR}}$.

Following [58] and by analogy to (27), let us write the sum of contributions coming from all processes of mutual electromagnetic dissociation:

$$\sigma_{\text{tot}}^{\text{MED}} = 2\pi \int_{b_c}^{\infty} dbb[1 - e^{-m_A(b)}]^2. \quad (37)$$

The RELDIS model results for the cross sections of mutual electromagnetic dissociation in the collisions of ultrarelativistic nuclei at the RHIC and LHC colliders will be given in the next subsections.

4.3. Nuclear Fragmentation Caused by Strong Interactions in Peripheral Collisions

Hadronic interactions of constituent nucleons in grazing nuclear collisions with impact parameters $b \sim R_{A_1} + R_{A_2}$ do not take place in each event. It is known that, because of the low peripheral density of matter, nuclei appear to be partially transparent to each other. At the same time, electromagnetic nuclear interactions can occur in such events. Finally, in a single combined event, both of these interactions can reveal themselves. For example, one can imagine that a collision of two nucleons in the overlap region of nuclear densities will lead to their knockout, while the electromagnetic interaction in the same event will result in pion photoproduction.

Let us consider the possibility of a smooth transition from the strong (hadronic) interaction dominating for $b < R_{A_1} + R_{A_2}$ to the electromagnetic one for $b > R_{A_1} + R_{A_2}$. Such a smooth transition is studied, in particular, in the soft-sphere model [88]. A similar approach was used in [58], where the cross section of nuclear fragmentation resulting from their strong or electromagnetic interaction (as well as from both these forces taken combined) was represented as follows:

$$\sigma = 2\pi \int_0^{\infty} dbb \times (\mathcal{P}^{\text{nuc}}(b) + \mathcal{P}^{\text{ED}}(b) - \mathcal{P}^{\text{nuc}}(b)\mathcal{P}^{\text{ED}}(b)), \quad (38)$$

where $\mathcal{P}^{\text{nuc}}(b)$ and $\mathcal{P}^{\text{ED}}(b)$ stand for the probabilities of hadronic and electromagnetic fragmentation (dissociation) at a given impact parameter b, respectively. Writing the limits of integration separately for each term, we obtain

$$\sigma = 2\pi \int_0^{b_c^{\text{nuc}}} dbb\mathcal{P}^{\text{nuc}}(b) + 2\pi \int_{b_c^{\text{ED}}}^{\infty} dbb\mathcal{P}^{\text{ED}}(b) - 2\pi \int_{b_c^{\text{ED}}}^{b_c^{\text{nuc}}} dbb\mathcal{P}^{\text{nuc}}(b)\mathcal{P}^{\text{ED}}(b). \quad (39)$$

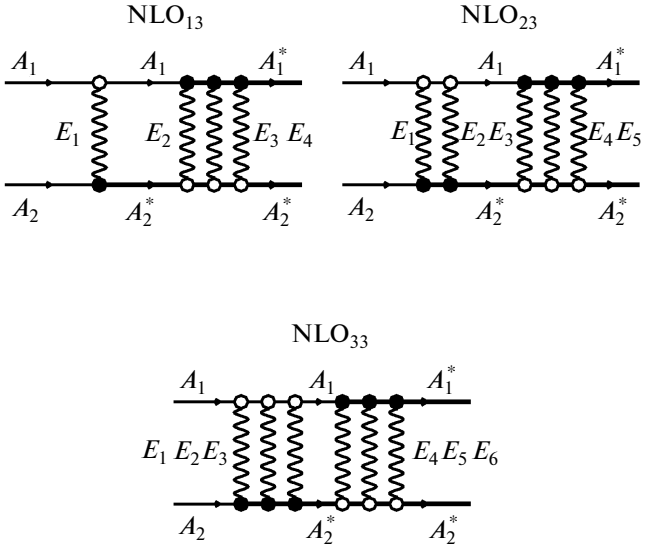

Fig. 15. Higher orders of mutual electromagnetic dissociation of nuclei accompanied by triple excitations. The diagrams of the processes with exchange of four (NLO_{13}), five (NLO_{23}), and six (NLO_{33}) photons are shown. Photon emission without changing a nuclear state is denoted by the light vertex, while photon absorption with nuclear excitation or particle production is shown by the dark one.

Here separate cutoff parameters for hadronic b_c^{nuc} and electromagnetic b_c^{ED} interactions were used.

Note that the following simplified expression is often used:

$$\sigma = \sigma^{\text{nuc}} + \sigma^{\text{ED}} = 2\pi \int_0^{b_c} dbb\mathcal{P}^{\text{nuc}}(b) + 2\pi \int_{b_c}^{\infty} dbb\mathcal{P}^{\text{ED}}(b), \quad (40)$$

in which a universal cutoff parameter is used within the range $b_c^{\text{ED}} < b_c < b_c^{\text{nuc}}$. This latter cutoff parameter b_c allows simplifying the expression in (39) by eliminating the last term. Then, the numerical results for (39) and (40) appear to be similar, as shown in [88] by comparing models that represent nuclei either as spheres with a diffuse surface or with a sharp boundary. Indeed, for heavy nuclei the difference between b_c^{ED}, b_c^{nuc}, and b_c is found to be less than 1 fm, thus making the last term in (39) small. Moreover, use of the expression (40) suggests that hadronic and electromagnetic interactions of nuclei take place strictly in different regions of the impact parameter b.

For b_c the known parameterization from [89] is used:

$$b_c = R_{\rm BCV}(A_1^{1/3} + A_2^{1/3} - X_{\rm BCV}(A_1^{-1/3} + A_2^{-1/3})). \quad (41)$$

The values $R_{\rm BCV} = 1.34$ fm and $X_{\rm BCV} = 0.75$ have been obtained in [89] from the best description of total cross sections of hadronic nuclear interactions by using the Glauber model. It is shown in [90] that the angular distributions of nuclear fragments produced in nucleus–nucleus collisions are rather sensitive to the choice of b_c. In the same paper, a good description of experimental data on the angular distributions was obtained by using parameterization (41).

In high-energy nuclear collisions at the LHC collider, intense hadron production is expected even with the small number of nucleon–nucleon collisions that takes place in peripheral hadronic interactions of nuclei. Note that the rapidities of such hadrons will be located in the central rapidity region, while the rapidities of neutrons from electromagnetic dissociation will be close to the initial rapidities of colliding nuclei. These differences will let us disentangle events with hadronic and electromagnetic dissociation occurring in the experiment.

The cross section of knocking out (an abrasion) a_1 nucleons from the A_1 nucleus that results from the collision with the A_2 nucleus is calculated by using the multiple scattering theory [91]:

$$\sigma^{\rm nuc}(a_1) = \binom{A_1}{a_1} 2\pi \int_0^\infty dbb[1 - P(b)]^{a_1}[P(b)]^{A_1 - a_1}. \quad (42)$$

Here $P(b)$ denotes the probability of nucleon preservation in a nucleus during collision with the impact parameter b, which is calculated by using the profile functions of both projectile $T_{A_1}(s)$ and target $T_{A_2}(|\vec{b} - \vec{s}|)$ nuclei:

$$P(b) = \frac{1}{A_1}\int d^2 s T_{A_1}(s) \times \exp[-\sigma_{NN} T_{A_2}(|\vec{b} - \vec{s}|)]. \quad (43)$$

The functions $T_A(s)$ are calculated as follows:

$$T_A(\vec{s}) = A \int_{-\infty}^{+\infty} dz \rho_A(\vec{s}, z), \quad (44)$$

and normalized by the condition $\int d^2 b T_A(b) = A$.

To evaluate the radial distribution of nuclear density in heavy nuclei, the Fermi distribution is used:

$$\rho_A(r) = \frac{\rho_0}{1 + \exp\left(\frac{r - r_0 A^{1/3}}{d}\right)}, \quad (45)$$

where the parameter r_0 defines the radius at which the nuclear density drops by half, $R_0 = r_0 \times A^{1/3}$, and $d = 0.54$ fm stands for the diffuseness of nuclear surface.

The results of calculations of the cross sections for a nucleon knockout from gold and lead nuclei in their collisions at the RHIC and LHC colliders are given in [32]. Here we cite only the cross section for a process in which nuclei undergo grazing peripheral interaction without a nucleon knockout, which is a consequence of partial transparency of the diffuse nuclear surfaces:

$$\sigma^{\rm nuc}(0) = 2\pi \int_0^\infty dbb[P(b)]^{A_1}. \quad (46)$$

In conclusion, we note that, in the vast majority of occurrences of hadronic fragmentation, the latter is in fact mutual.

4.4. Multiple Excitations of Giant Resonances in Nuclear Collisions at the LHC

Let us consider the conditions in which multiple excitations of giant resonances take place in the collisions of relativistic nuclei. The cross sections of a single and mutual electromagnetic dissociation are written in the general form

$$\sigma^{\rm (S,\,M)ED} = 2\pi \int_{b_c}^\infty dbb\mathcal{P}^{\rm (S,\,M)ED}(b), \quad (47)$$

as integrals of the probabilities of the corresponding processes $\mathcal{P}^{\rm SED}(b)$ and $\mathcal{P}^{\rm MED}(b)$ as a function of the impact parameter b. The dependences for $\mathcal{P}^{\rm MED}(b)$ are given by the expressions for leading and higher orders (34)–(36), while the expressions for $\mathcal{P}^{\rm SED}(b)$ follow directly from (18), (23), and (26) after interchanging the order of integration in the latter. Note that Eq. (47) corresponds to the nuclear model with a sharp boundary and abrupt transition from the region of strong interaction to that of electromagnetic interaction at the impact parameter b_c. For comparison, when a nuclear model with a diffuse boundary is used, the cross section can be written as

$$\sigma^{\rm (S,\,M)ED} = 2\pi \int_0^\infty dbb[P(b)]^A \mathcal{P}^{\rm (S,\,M)ED}(b), \quad (48)$$

which follows from (46) written for the case of nuclear collisions without a nucleon knockout from nuclei.

The product $[P(b)]^A \mathcal{P}^{\rm (S,\,M)ED}(b)$ in (48) is displayed in Fig. 16 for single and mutual electromagnetic dissociation in the LO and NLO processes considered above. The use of a nuclear model with a sharp boundary instead of one with a diffuse one alters the total cross section $\sigma^{\rm (S,\,M)ED}$ by several percent, which is within the error caused by the uncertainties in the cross sections of photonuclear reactions. The main

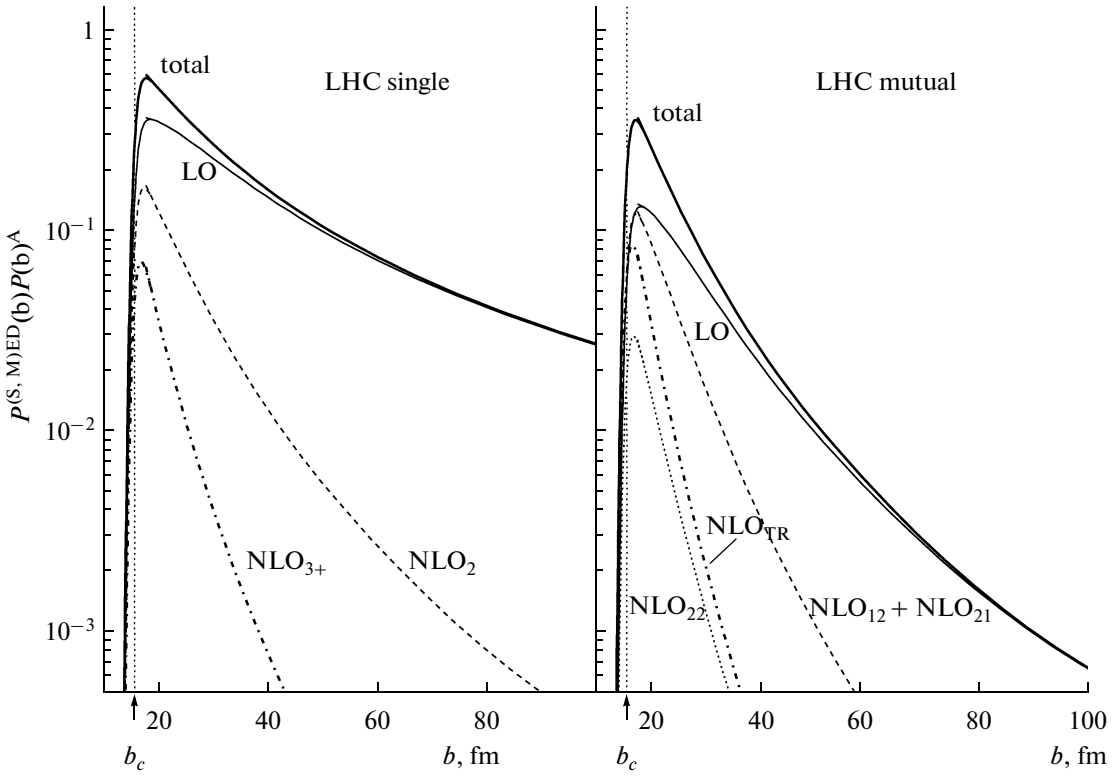

Fig. 16. Probabilities of a single (to the left) and mutual (to the right) electromagnetic dissociation in the leading (LO) and next-to-leading (NLO) orders as a function of the impact parameter b in PbPb collisions at energy of 2.75 + 2.75 A TeV at the LHC [14]. The results of both RELDIS and abrasion models for nuclei with a diffuse boundary are shown. The bold solid curve corresponds to the sum of all processes the individual contributions of which are depicted by different curves with the corresponding notation. The value of $b_c = 15.54$ fm related to the nuclear model with a sharp boundary is marked on the plot as well.

contribution to σ^{MED} comes from electromagnetic collisions of nuclei with small impact parameters $b \sim b_c$, in which the probability for an equivalent photon to be absorbed is high. In such collisions the probabilities for two and more photons to be absorbed by one or two nuclei are significantly high. The mutual dissociation probabilities decrease considerably faster with b increasing than the single dissociation probabilities (see Fig. 16). Therefore, the selection of events corresponding to the mutual dissociation processes allows one to isolate events with small impact parameters $b \sim b_c$.

As is shown in Fig. 16, the relative contributions of NLO processes to the cross section of mutual dissociation are considerably higher than analogous ones to the cross section of single dissociation. Indeed, the sum $NLO_{12} + NLO_{21}$ is almost equal to the LO at $b \sim b_c$. In addition, in this particular region of small impact parameters, the contributions to mutual dissociation coming from the processes of triple excitations NLO_{TR} are comparable to that of the leading order. At the same time, with b increasing, all the NLO contributions decrease more rapidly than does the LO one; therefore, the NLO cross sections presented in Table 4 turn out to be smaller than the LO ones.

The values of LO cross sections, along with the additional contributions from NLO_{12}, NLO_{22}, and NLO_{TR} processes to the total cross section of mutual electromagnetic dissociation calculated under the condition $f(E, i) = f(E, j) = 1$ in the expressions for $\sigma^{MED}(i|j)$ are given in Table 4. The leading order contribution is ~63% of σ^{MED}(tot) in the collisions of lead nuclei at the LHC energy. The sum of the contributions coming from double excitations amounts to ~28% of the total cross section. The remaining part of the cross section for mutual electromagnetic dissociation (~9%) corresponds to exotic nuclear excitations,

Table 4. Leading order (LO) cross sections (in units of barns) and contributions of NLO processes to the total cross section of mutual electromagnetic dissociation in PbPb collisions at an energy of 2.75 + 2.75 A TeV at the LHC [14]

σ^{MED}_{LO}	$\sigma^{MED}_{NLO_{12}} + \sigma^{MED}_{NLO_{21}}$	$\sigma^{MED}_{NLO_{22}}$	$\sigma^{MED}_{NLO_{TR}}$	σ^{MED}_{tot}
3.92	1.50	0.23	0.56	6.21

Table 5. Cross sections of mutual electromagnetic dissociation of lead nuclei in collisions at the LHC at an energy of 2.75 + 2.75 A TeV [14]. Symbols X and Y denote undetected particles emitted by nuclei in addition to neutrons, while $\mathcal{D}$ corresponds to an arbitrary channel of a partner-nucleus dissociation, $f(E, i) = 1$. RELDIS results are given for the leading order (a) and the sum of the leading order and next-to-leading contributions (b)

Final state	σ_{LO} (mb) (a)	$\sigma_{LO} + \sigma_{NLO_{12}} + \sigma_{NLO_{21}} + \sigma_{NLO_{22}}$ (mb) (b)
$(1nX\|1nY)$	750	805
$(1nX\|\mathcal{D})$	1698	2107
$(2nX\|\mathcal{D})$	443	654
$(3nX\|\mathcal{D})$	241	465

in which three and more photons are absorbed by at least one of the colliding nuclei.

The relations between the cross sections of nuclear excitation of the leading and next-to-leading orders presented in Table 4 differ favorably from the analogous ones that are observed in electromagnetic nuclear excitations in collisions with fixed targets at energies of several gigaelectronvolts per nucleon [23, 92]. In the latter case, the detection of double excitations is an important tool for investigating a nuclear structure; however, the double excitations registered in such experiments are dozens of times less likely to occur than single ones. On the contrary, as follows from Table 4, more than one-third of events of mutual dissociation are related with multiple excitations. Therefore, an experimental study of mutual electromagnetic dissociation at the LHC will provide important information about double and triple excitations of giant resonances. The data on triple excitations will be a new piece of knowledge, since these excitations of giant resonances are still largely unexplored. The first theoretical results for energy and width of such exotic excitations are given in [93].

At the LHC the multiple nuclear excitations can be studied by detecting neutrons emitted in the forward direction, even if the resolution of ZDC calorimeters does not allow one to determine the exact number of neutrons emitted by one of the nuclei. Indeed, let us suppose that one of the nuclei has dissociated, but the exact composition of fragments is not known. An arbitrary decay mode of such a nucleus is denoted by $\mathcal{D}$ and the value $f(E, i) \equiv 1$ is taken. In this case the inclusive cross sections $\sigma^{MED}(1nX|\mathcal{D})$, $\sigma^{MED}(2nX|\mathcal{D})$, and $\sigma^{MED}(3nX|\mathcal{D})$, corresponding to emission of one, two, and three neutrons by another nucleus, can be considered. The symbol X expresses the fact that, in addition to a certain number of neutrons, other undetected particles are emitted.

The partial cross sections for the channels with mutual electromagnetic dissociation of lead nuclei at the LHC are presented in Table 5. The corresponding branching ratios for the channels $f(E, 1nX)$, $f(E, 2nX)$, and $f(E, 3nX)$ were calculated by simulating dissociation of a nucleus (by means of the Monte Carlo procedure) after absorption by the latter of a photon with energy E. The expression in (33) comprises the branching ratios of the corresponding channels for each nucleus, with the factor $\exp[-m_A(b)]$ taken the same for both partners as $A_1 = A_2$. In particular, the cross sections $\sigma^{MED}(1nX|1nY)$ are smaller than $\sigma^{MED}(1nX|\mathcal{D})$ because of taking into account the branching ratios $f(E, 1nX)$ and $f(E, 1nY)$ for each nucleus.

The relative contribution of the next-to-leading order processes differs sizably for channels with emission of one, two, and three neutrons. Such a contribution to $\sigma^{MED}(1nX|1nY)$ turns out to be rather small, ~7%. On the other hand, when next-to-leading order processes are taken into account $\sigma^{MED}(3nX|\mathcal{D})$ increases almost twice as much due to the effect of double excitations of giant resonances. Since the mean excitation energy of a giant dipole resonance in gold and lead nuclei is ~13–14 MeV, the double excitations contribute 26–28 MeV, thus going beyond the triple-neutron emission threshold. This explains the relatively small changes in the cross sections of $1n$ and $2n$ with the next-to-leading order corrections taken into account as compared with $3n$ cross sections. Thus, the measurements of $3n$ cross sections at the LHC and their comparison with theoretical predictions enable one to estimate the probability of multiple excitations of giant resonances in nuclei.

5. ELECTROMAGNETIC DISSOCIATION OF NUCLEI AND RHIC AND LHC LUMINOSITY MONITORING

As shown above in Subsections 3.4, 3.5, and 3.6, the RELDIS model successfully describes experimental data on electromagnetic dissociation of heavy nuclei on fixed targets at energies from 30 to 158 A GeV. Owing to the success of the model, one can look forward to the reliable predictions at even higher energies accessible at the RHIC and LHC colliders.

At those colliders events of mutual electromagnetic dissociation of nuclei take place at the beam crossing point. After that point the nuclear fragments produced by electromagnetic dissociation can be separated according to their values of Z/A by applying the magnetic field. The protons and charged nuclear fragments

Table 6. Cross sections for channels of mutual electromagnetic dissociation of gold nuclei with emission of several neutrons [32]. RELDIS results are given for colliding beams at the RHIC: for the leading order (a) and for the sum of leading and next-to-leading orders (b). Other particles emitted by either nuclei in addition to neutrons are collectively denoted as X and Y, respectively, while $\mathcal{D}$ stands for an arbitrary channel of electromagnetic dissociation

	cross section (mb)	(a) LO	(b) LO + NLO
65 + 65 A GeV	$\sigma^{\mathrm{MED}}(1nX\|1nY)$	612	659
	$\sigma^{\mathrm{MED}}(1nX\|\mathcal{D})$	1244	1502
	$\sigma^{\mathrm{MED}}(2nX\|\mathcal{D})$	330	446
	$\sigma^{\mathrm{MED}}(3nX\|\mathcal{D})$	148	274
100 + 100 A GeV	$\sigma^{\mathrm{MED}}(1nX\|1nY)$	607	652
	$\sigma^{\mathrm{MED}}(1nX\|\mathcal{D})$	1257	1518
	$\sigma^{\mathrm{MED}}(2nX\|\mathcal{D})$	341	461
	$\sigma^{\mathrm{MED}}(3nX\|\mathcal{D})$	155	284

propagate far in the forward direction close to the initial beam trajectory inside the accelerator setup, while free neutrons escape outside after a dipole magnet.

All of the RHIC experiments and the ALICE experiment at the LHC are equipped with zero-degree calorimeters that are intended for detection of particles emitted strictly in the forward directions of either beams. Since ZDCs were specifically designed to detect neutrons [9, 28, 58, 61], the semi-inclusive cross sections of neutron emission $\sigma^{\mathrm{MED}}(i|j)$ will further be dealt with. Here i and j denote the corresponding channels with emission of a given number of neutrons: $1nX$, $2nX$, $3nX$, ..., accompanied by other undetected particles collectively marked by X or Y, such as protons, mesons, or nuclear fragments.

In Subsection 3.4 the RELDIS model was shown to well describe the experimental data on emission of one or two neutrons in electromagnetic dissociation of lead and gold nuclei. As this model predicts, the protons are most frequently emitted along with neutrons in electromagnetic dissociation of heavy nuclei, thus decreasing charges of interacting nuclei. It is shown in Subsection 3.5 that the model well describes also the experimental data on proton emission; therefore, it can be expected that the cross sections $\sigma^{\mathrm{MED}}(1nX|1nY)$, $\sigma^{\mathrm{MED}}(1nX|2nY)$, and $\sigma^{\mathrm{MED}}(2nX|2nY)$ for channels with proton presence will reliably be calculated at even higher energies.

The detection of events with mutual electromagnetic dissociation of nuclei makes it possible to monitor the collider luminosity online during its run. The method of monitoring a nucleus–nucleus collider proposed in [58] allows one to determine the collider luminosity by measuring the event rate for mutual electromagnetic dissociation R^{MED}:

$$L = \frac{R^{\mathrm{MED}}}{\sigma^{\mathrm{MED}}}, \qquad (49)$$

if the cross section of mutual electromagnetic dissociation σ^{MED} is known (theoretically predicted) with sufficient accuracy.

5.1. Mutual Electromagnetic Dissociation of Nuclei at the RHIC Collider

The cross sections of mutual electromagnetic dissociation of gold nuclei with neutron emission are presented in Table 6 for two values of the collision energy at the RHIC. With the beam energy increased from 65 to 100 GeV per nucleon absolute values of the cross sections slightly increase. Simultaneously, the probabilities redistribute in favor of channels with higher neutron multiplicity.

Taking into account the next-to-leading order processes results in the increase of $\sigma^{\mathrm{MED}}(3nX|\mathcal{D})$ almost twice as much. For comparison, $\sigma^{\mathrm{MED}}(1nX|1nY)$ increases by only 7% when NLO corrections are taken into account. Just as in the case of lead nuclei colliding at the LHC considered above in Subsection 4.4, the multiphoton excitations of GR substantially increase the probability of triple-neutron emission.

The double excitations of GDR have been studied in nuclear collisions at low and intermediate energies [22–24]. However, only with the advent of the RHIC era did it become possible to study the multiple excitations of ultrarelativistic nuclei in the processes of mutual electromagnetic dissociation. The key point here is how close the probability distribution of multiple excitations is to a Poisson distribution and how well it reproduces the excitations of a harmonic oscillator.

To determine contributions of multiple nuclear excitations (including those with energies higher than GR) it was proposed in [32] to measure the ratios $\sigma^{\mathrm{MED}}(2nX|\mathcal{D})/\sigma^{\mathrm{MED}}(1nX|1nY)$ and $\sigma^{\mathrm{MED}}(3nX|\mathcal{D})/\sigma^{\mathrm{MED}}(1nX|1nY)$. In the case of suppressing multiple nuclear excitations (in particular, deviations of the probability distribution of multiphoton processes from an expected Poisson one), the

Table 7. Stability of cross sections for mutual electromagnetic dissociation of gold nuclei at energy of 100 + 100 A GeV against probability of direct emission in the 1n channel (P_n^{dir}), variations in photonuclear cross sections, and NLO corrections [32]. All the calculations done within the RELDIS model, except for version (b), use their own model for photonuclear reactions. In version (b) the photonuclear cross sections from the GNASH model are used. Results for version (e) are presented in boldface as the most realistic ones and recommended for use. For comparison, the cross section $\sigma^{\mathrm{MED}}(1n|1n)$ from [58] is given

Cross section (mb)	$E_\gamma \le 24$ MeV, LO	$E_\gamma \le 140$ MeV, LO		Entire range E_γ LO + NLO	
	(a) RELDIS $P_n^{\mathrm{dir}} = 0$	(b) GNASH	(c) RELDIS $P_n^{\mathrm{dir}} = 0$	(d) RELDIS $P_n^{\mathrm{dir}} = 0$	(e) RELDIS $P_n^{\mathrm{dir}} = 0.31$
$\sigma^{\mathrm{MED}}(1nX\|1nY)$	437 445 [58]	430	467	549	**652**
$\sigma^{\mathrm{MED}}(1nX\|2nY) + \sigma^{\mathrm{MED}}(2nX\|1nY)$	205	221	262	439	**388**
$\sigma^{\mathrm{MED}}(2nX\|2nY)$	21	28	38	87	**60**
$\sigma^{\mathrm{MED}}(LMN)$	663	679	767	1075	**1100**

experimental ratios of the cross sections from Table 6 will be less than those predicted by theory.

The nucleus–nucleus collider luminosity monitor based on neutron detection from each beam [28, 58, 61] requires reliable calculations of the cross sections for the channels of mutual electromagnetic dissociation with neutron emission. Therefore, it is necessary to estimate the sensitivity of the calculated cross sections to the variations in input parameters.

Table 7 shows the sensitivity of the cross sections of mutual electromagnetic dissociation to those of photonuclear reactions used in the calculations. Let us remember (see Subsection 3.3) that the RELDIS model can use both its own model for photonuclear reactions (see Subsection 2.2) and photonuclear cross sections calculated using the GNASH model [64]. In the first version, two different values for the probability of direct neutron emission in the 1n channel were used: $P_n^{\mathrm{dir}} = 0$ and 0.31. The calculations were carried out within three ranges of virtual photon energies: $E_\gamma \le$ 24 MeV, $E_\gamma \le 140$ MeV, and the entire range of E_γ.

In Table 7, besides the cross sections of the one- or two-neutron emission, a low-multiplicity neutron emission cross section (LMN) can be found, which is calculated according to the following formula:

$$\sigma^{\mathrm{MED}}(LMN) = \sigma^{\mathrm{MED}}(1nX|1nY) + \sigma^{\mathrm{MED}}(1nX|2nY) + \sigma^{\mathrm{MED}}(2nX|1nY) + \sigma^{\mathrm{MED}}(2nX|2nY).$$

It is seen from this table that, first, the semi-inclusive cross section $\sigma^{\mathrm{MED}}(1nX|1nY) = 437$ mb that accounts for photoabsorption in the vicinity of a giant resonance appears to be close to the quantity $\sigma^{\mathrm{MED}}(1n|1n) = 445$ mb from [58] obtained with the same constraint $E_\gamma \le 24$ MeV. However, within a wider range of E_γ, $\sigma^{\mathrm{MED}}(1nX|1nY) > \sigma^{\mathrm{MED}}(1n|1n)$; therefore, the cross section of strictly one neutron emission, $\sigma^{\mathrm{MED}}(1n|1n)$, should not be used in place of $\sigma^{\mathrm{MED}}(1nX|1nY)$ to monitor the RHIC luminosity.

Second, if the energies are bounded from the above $E_\gamma \le 140$ MeV, then the values calculated by using the photonuclear cross sections from the GNASH model turn out to be close to the results obtained by using the cross sections from the RELDIS' photonuclear model. Note that the difference in RELDIS results for $E_\gamma \le 24$ and $E_\gamma \le 140$ MeV is due to the contribution to 1n and 2n emissions caused by quasi-deuteron photoabsorption (see Subsection 2.2). Despite the fact that photoabsorption in the GR region contributes significantly to the cross sections considered, their values can only be reliably calculated while considering the entire range of E_γ.

Third, the calculations with quasi-deuteron absorption and reactions above the pion photoproduction threshold taken into account in addition to the GDR excitation increase $\sigma^{\mathrm{MED}}(1nX|1nY)$ by approximately 25%. At the same time, $\sigma^{\mathrm{MED}}(1nX|2nY)$ and $\sigma^{\mathrm{MED}}(2nX|2nY)$ almost double and triple, respectively, compared with the calculations performed for $E_\gamma \le$ 24 MeV.

Fourth, it is important to note that the calculations with $P_n^{\mathrm{dir}} = 0$ and 0.31 yield differences for the 1n and 2n cross sections at the level of 10–40%, while $\sigma^{\mathrm{MED}}(LMN)$ changes only slightly. This latter cross section is sufficiently large, $\sigma^{\mathrm{MED}}(LMN) \sim 1100$ mb, and can be used to monitor the RHIC luminosity. The systematic error in the calculations of $\sigma^{\mathrm{MED}}(LMN)$ is ~5%.

Table 8 shows the sensitivity of the cross sections of mutual dissociation in electromagnetic and nuclear interactions to the value of the boundary impact parameter b_c parameterized according to (41). With b_c varied within 14.5 to 16 fm (by 5%), the electromagnetic dissociation cross sections change by 3–8%. Such variations in b_c shift the point that separates the regions with strong and electromagnetic interactions

Table 8. Stability of cross sections for mutual dissociation of gold nuclei at energy of 100 + 100 A GeV in electromagnetic and nuclear interactions against variations in the boundary impact parameter b_c [32]. Results of both RELDIS and abrasion models are presented. The values of option (b) recommended for use and presented in boldface

Cross section (mb)	(a) $R_{BCV} = 1.27$ $b_c = 14.45$ fm	(b) $R_{BCV} = 1.34$ $b_c = 15.25$ fm	(c) $R_{BCV} = 1.41$ $b_c = 16.05$ fm
$\sigma^{MED}(1nX\|1nY)$	677	**652**	629
$\sigma^{MED}(1nX\|2nY) + \sigma^{MED}(2nX\|1nY)$	417	**388**	374
$\sigma^{MED}(2nX\|2nY)$	62	**60**	57
$\sigma^{MED}(LMN)$	1156	**1100**	1060
$\sigma^{nuc}(1nX\|1nY)$	379	**371**	390
$\sigma^{nuc}(1nX\|2nY) + \sigma^{MED}(2nX\|1nY)$	240	**224**	259
$\sigma^{nuc}(2nX\|2nY)$	141	**142**	151
$\sigma^{nuc}(LMN)$	760	**737**	800
$\sigma^{MED}(LMN) + \sigma^{nuc}(LMN)$	1916	**1837**	1860

of nuclei above or below the impact parameter region where diffuse nuclear densities overlap. In other words, assuming first $b_c \approx b_c^{ED}$, then $b_c \approx b_c^{nuc}$, and analyzing the difference in the final results, we can justify the use of simplified expression (40) instead of (39).

In particular, with b_c increasing, all the cross sections of electromagnetic dissociation ($1nX$, $1nY$), ($1nX$, $2nY$), ($2nX$, $2nY$), and $\sigma^{MED}(LMN)$ become smaller. The changes in the cross sections of nuclear interactions are more evident and opposite in behavior; these cross sections increase by 5–15%. Finally, it can be noted that the spread in $\sigma^{MED}(LMN)$ values turns out to be less than the changes in the partial cross sections, while the sum $\sigma^{MED}(LMN) + \sigma^{nuc}(LMN)$ varies only by 1–4%.

In concluding our consideration of the sensitivity of the calculation results to variations in the input parameters, we note that, for the collisions of gold nuclei at the RHIC, $\sigma^{MED}(LMN) = 1100$ and $\sigma^{nuc}(LMN) = 737$ mb are considerably more stable compared with $\sigma^{MED}(1nX|1nY)$, $\sigma^{MED}(1nX|2nY)$, and other partial cross sections.

It can be expected that, as a result of a collision of two identical nuclei, they will be disintegrated in about equal measure. This picture of collisions is valid for strongly interacting nuclei with pairwise interactions of nucleons at the initial stage. One nucleon from each partner-nucleus takes part in such interactions; therefore, nuclear dissociation (fragmentation) is always mutual.

On the contrary, electromagnetic interactions can result in events ($1nX|5nY$) or even ($1nX|10nY$). This feature of mutual electromagnetic dissociation as compared with the strong interactions of nuclei is shown in Fig. 17, where the cross sections for emission of one, two, and three neutrons in one arm of a ZDC are presented. For example, the events ($1nX|10nY$) are virtually absent in nuclear interactions, whereas the yields of asymmetric electromagnetic events ($1nX|10nY$) are 1–5% of the yields corresponding to the main channel ($1nX|1nY$).

According to the RELDIS model, the processes of electromagnetic dissociation of each of the partner-nuclei proceed independently of each other (see Subsection 4.1). Therefore, the numbers of neutrons n_1 and n_2 emitted by each of the nuclei do not correlate and asymmetric dissociation events are possible along with symmetric ones. Single electromagnetic dissociation can be regarded as an extremely asymmetric case of mutual electromagnetic dissociation. In contrast, nuclear fragmentation in peripheral collisions under impact of strong interactions, which is interpreted in the context of the abrasion model (Subsection 4.3), reveals a correlation among the number of nucleons emitted by each of the nuclei: $z_1 + n_1 \sim z_2 + n_2$.

These features are illustrated in Fig. 18, where the cross sections of electromagnetic and nuclear dissociation at the RHIC collider are presented. Since $1n$ and $2n$ emissions in electromagnetic dissociation of nuclei dominate due to the processes of GDR excitation and quasi-deuteron absorption, the corresponding rows and columns contain maximal values of the cross sections. Simultaneous emission of only one neutron by each of the partner-nuclei is the most probable process of mutual electromagnetic dissociation, although its cross section accounts for only ~17% of the total one. The rest of the former is due to various asymmetric processes, with GDR excited in one of the nuclei and a photon with energy higher than that of GDR absorbed by another nucleus, thus leading to emission of several neutrons. As follows from Fig. 18, the probabilities for three and more neutrons to be emitted appear to be substantially smaller than the $1n$ and $2n$ cross sections, such processes being induced by high-energy photons are widely distributed across the plot shown in Fig. 18.

The processes of mutual electromagnetic dissociation, which proceed without neutrons emitted by one

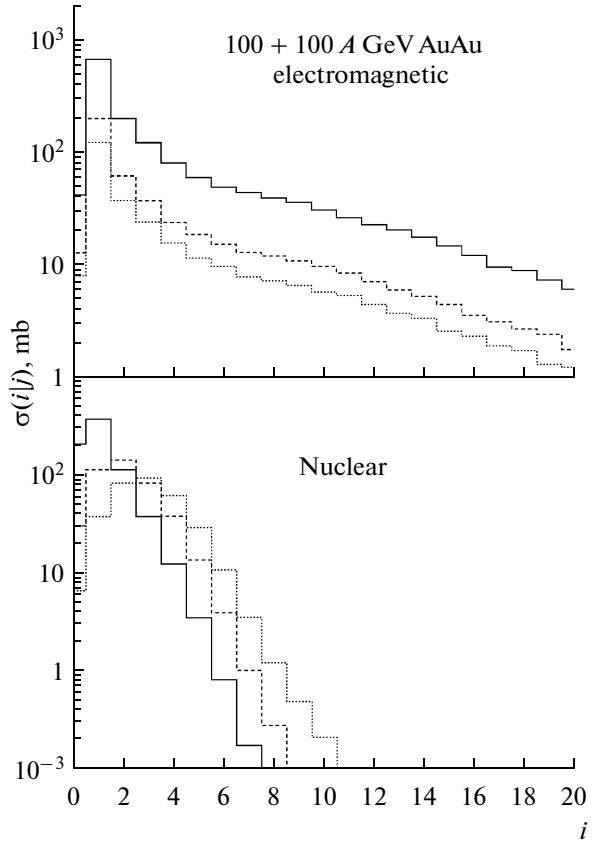

Fig. 17. Cross sections of mutual electromagnetic dissociation $\sigma^{MED}(i|j)$ (upper panel) and those of nuclear fragmentation $\sigma^{nuc}(i|j)$ (lower panel) for emission of a given number of neutrons ($i = 0nX$, $1nX$, $2nX$, ... $20nX$, $j = 1nY$, $2nY$, $3nY$) by each nucleus in collisions of gold nuclei at an energy of 100 + 100 A GeV [32]. Histograms shown by solid, dashed, and dotted lines correspond to cross sections with $j = 1nY$, $2nY$, $3nY$, respectively.

or two nuclei, complement the cross-section plot displayed in Fig. 18. The cross sections of such processes are too small, which is yet another distinction between electromagnetic dissociation and peripheral nuclear fragmentation. The peripheral nuclear interactions lead with appreciable probability to the loss of protons without neutron emission.

In Table 9 the ratios of the cross sections for mutual dissociation measured in [94] in the collisions of gold nuclei at the RHIC are presented. These experimental results are compared with theoretical values calculated by using the RELDIS (σ^{MED}) and abrasion (σ^{nuc}_{tot}) models. In general, experimental results are well described by the theory. As was noted above, the cross sections of $1n$ channels increase by 15–20% if the existence of additional direct mechanism of single-neutron emission is assumed. The results presented in Table 9 are obtained by assuming $P_n^{dir} = 0.31$, which is justified by comparing calculations and experiment at energies below those of the RHIC (see Subsection 3.4). Such a choice of P_n^{dir} may be a reason for the overestimation of $1n$ emission seen in Table 9 with respect to experiment. It should once again be emphasized that cross sections $\sigma^{MED}(LMN)$ are more stable against the choice in the calculation parameters as compared with $1n$ and $2n$ cross sections taken separately.

5.2. Mutual Electromagnetic Dissociation of Nuclei at the LHC Collider

The reliability of the RELDIS model is confirmed by the good agreement between theoretical results and experimental data [72–75] on single electromagnetic dissociation of gold and lead nuclei in their collisions with various nuclei at the energies of the CERN SPS. In addition, it was found that the model results are in good agreement with the data on mutual nuclear dissociation obtained at the RHIC [94] (see Subsection 5.1). All these give credit to using the model in calculations to be carried out at even higher LHC energies.

As a result of ultraperipheral nuclear interactions, the nuclear fragments are produced at the LHC beam crossing points. In addition, electromagnetic dissociation may as well take place on the residual gas nuclei [28]. Most such fragments have typical charges and masses close to those of the beam nuclei; therefore, their trajectories in the magnetic field of the accelerator pass close to that of the beam. This complicates the separation of such fragments from the beam nuclei by employing a set of collimators, thus leading to probable contamination of the accelerator construction elements by these fragments and, therefore, causing a local thermal load on the former. This additional thermal load may turn out to be critical for superconducting magnets of the accelerator and cause a loss of their superconductivity. Analogous phenomena at the RHIC collider were discussed in [29]. To estimate the impact of nuclear fragments produced in electromagnetic dissociation of beam nuclei on the LHC magnets, tables of fragment yields predicted by the RELDIS and abrasion–ablation models were used in [95, 96].

Reliable predictions for the cross sections of mutual electromagnetic dissociation of nuclei at the LHC are required to monitor the collider luminosity. The cross sections of mutual electromagnetic dissociation of lead nuclei in ultraperipheral collisions at the LHC are given in Table 10. Similarly to the calculations done at the RHIC energy (see Subsection 5.1), two independent models of photonuclear reactions, GNASH [64] and RELDIS [32], have been used to calculate the branching ratios $f(E, i)$. In order to test the stability of calculation results, two values for the probability of direct neutron emission were used in the RELDIS model, $P_n^{dir} = 0$ and 0.26, and, then, the results were compared with each other.

The cross sections for one or two neutron emission presented in Table 10 are obtained by using sev-

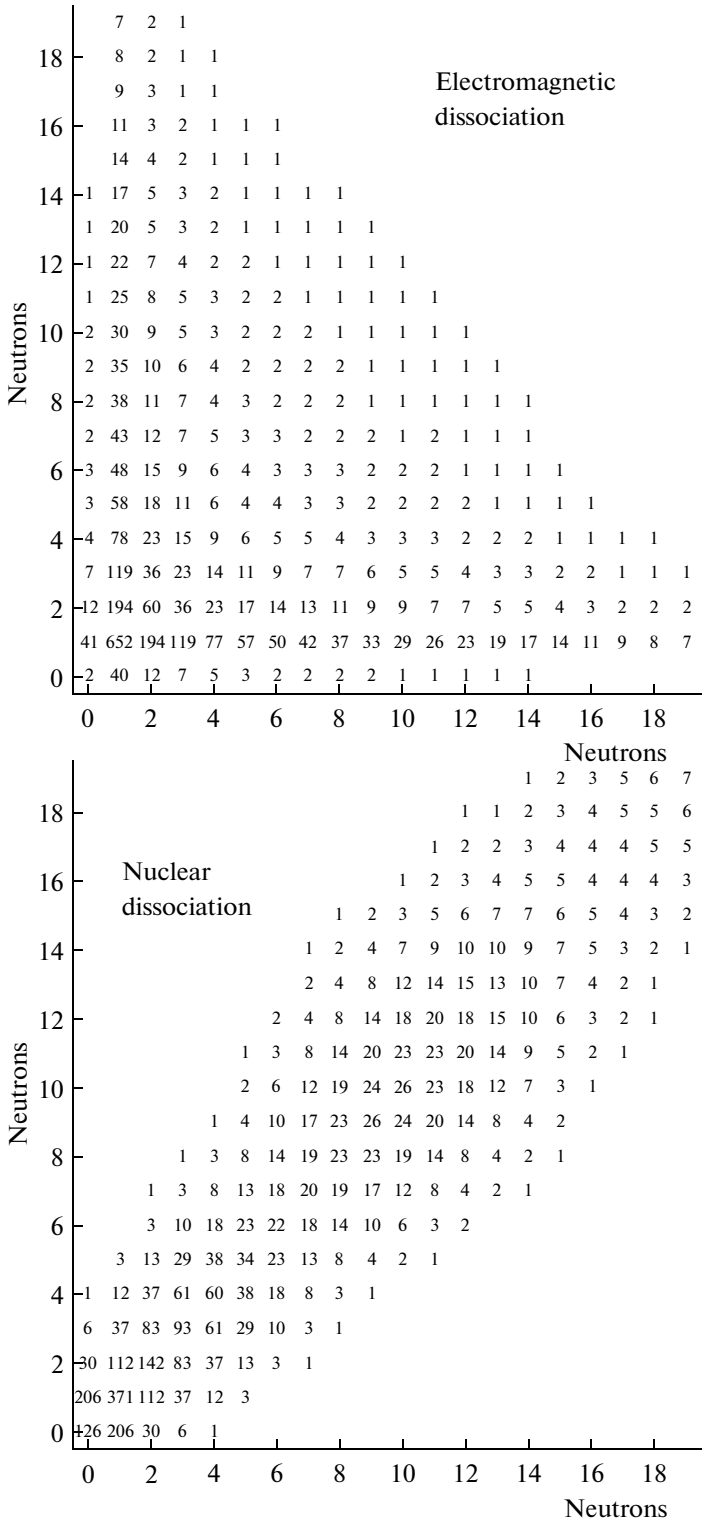

Fig. 18. Cross sections of mutual electromagnetic dissociation of gold nuclei $\sigma^{MED}(i|j)$ (millibarns) accompanied by emission of a certain number of neutrons ($i, j = 0nX, 1nX, ..., 19nX$) (upper panel) and analogous cross sections $\sigma^{nuc}(i|j)$ for nuclear fragmentation (lower panel) [32]. The values of partial cross sections obtained by using the RELDIS and abrasion models correspond to the energy of $100 + 100\ A$ GeV.

Table 9. Ratios of the cross sections of mutual dissociation in AuAu collisions at the energy of 65 + 65 A GeV [14]. Experimental data are obtained in the experiments PHENIX, PHOBOS, and BRAHMS at the RHIC [94]. Absolute values of the cross sections and their ratios are calculated by using the RELDIS and abrasion models

	PHENIX	PHOBOS	BRAHMS	Theory
σ_{tot}^{MED} (b)	–	–	–	3.6
σ_{tot}^{nuc} (b)	–	–	–	7.29
$\sigma_{tot} = \sigma_{tot}^{MED} + \sigma_{tot}^{nuc}$ (b)				10.89
$\frac{\sigma_{tot}^{nuc}}{\sigma_{tot}}$	0.661 ± 0.014	0.658 ± 0.028	0.68 ± 0.06	0.669
$\frac{\sigma^{MED}(1nX\|\mathcal{D})}{\sigma_{tot}}$	0.117 ± 0.004	0.123 ± 0.011	0.121 ± 0.009	0.138
$\frac{\sigma^{MED}(1nX\|1nY)}{\sigma^{MED}(1nX\|\mathcal{D})}$	0.345 ± 0.012	0.341 ± 0.015	0.36 ± 0.02	0.439
$\frac{\sigma^{MED}(2nX\|\mathcal{D})}{\sigma^{MED}(1nX\|\mathcal{D})}$	0.345 ± 0.014	0.337 ± 0.015	0.35 ± 0.03	0.297
$\frac{\sigma^{MED}(1nX\|1nY)}{\sigma_{tot}}$	0.040 ± 0.002	0.042 ± 0.003	0.044 ± 0.004	0.061

Table 10. Cross sections of mutual electromagnetic dissociation of lead nuclei (in millibarns) at the energy of 2.75 A + 2.75 A TeV at the LHC [14]. Results are obtained by using the GNASH and RELDIS models of photonuclear reactions for the leading and next-to-leading orders. Results of the optimum option (e) shown in boldface are recommended for further use. For comparison, the value for $\sigma_{LO}^{MED}(1n|1n)$ from [58] corresponding to $E_\gamma \le 24$ MeV is quoted in parentheses

Dissociation channel	GR region $E_\gamma \le 24$ MeV	QD absorption $E_\gamma \le 140$ MeV		All processes	
	σ_{LO}^{MED}	σ_{LO}^{MED}		$\sigma_{LO}^{MED} + \sigma_{NLO_{12}}^{MED} + \sigma_{NLO_{21}}^{MED} + \sigma_{NLO_{22}}^{MED}$	
	(a) RELDIS $P_n^{dir} = 0$	(b) GNASH	(c) RELDIS $P_n^{dir} = 0$	(d) RELDIS $P_n^{dir} = 0$	(e) RELDIS $P_n^{dir} = 0.26$
$(1nX\|1nY)$	519 (533)	488	544	727	**805**
$(1nX\|2nY) + (2nX\|1nY)$	154	220	217	525	**496**
$(2nX\|2nY)$	11	24	22	96	**77**
LMN	684	732	783	1348	**1378**

eral calculation options for different ranges of equivalent photon energy, $E_\gamma \le E_{max}$, with the upper bound corresponding to the upper limit of integration over the energy in Eq. (19). The results are given for the region of giant resonances $E_\gamma \le 24$ MeV, for energies within the range of quasi-deuteron absorption $E_\gamma \le$ 140 MeV, as well as for the entire range. Besides cross sections of the channels with one or two neutron emission, it is appropriate to consider the LMN cross section:

$$\sigma^{MED}(LMN) = \sigma^{MED}(1nX|1nY) + \sigma^{MED}(1nX|2nY) + \sigma^{MED}(2nX|1nY) + \sigma^{MED}(2nX|2nY), \quad (50)$$

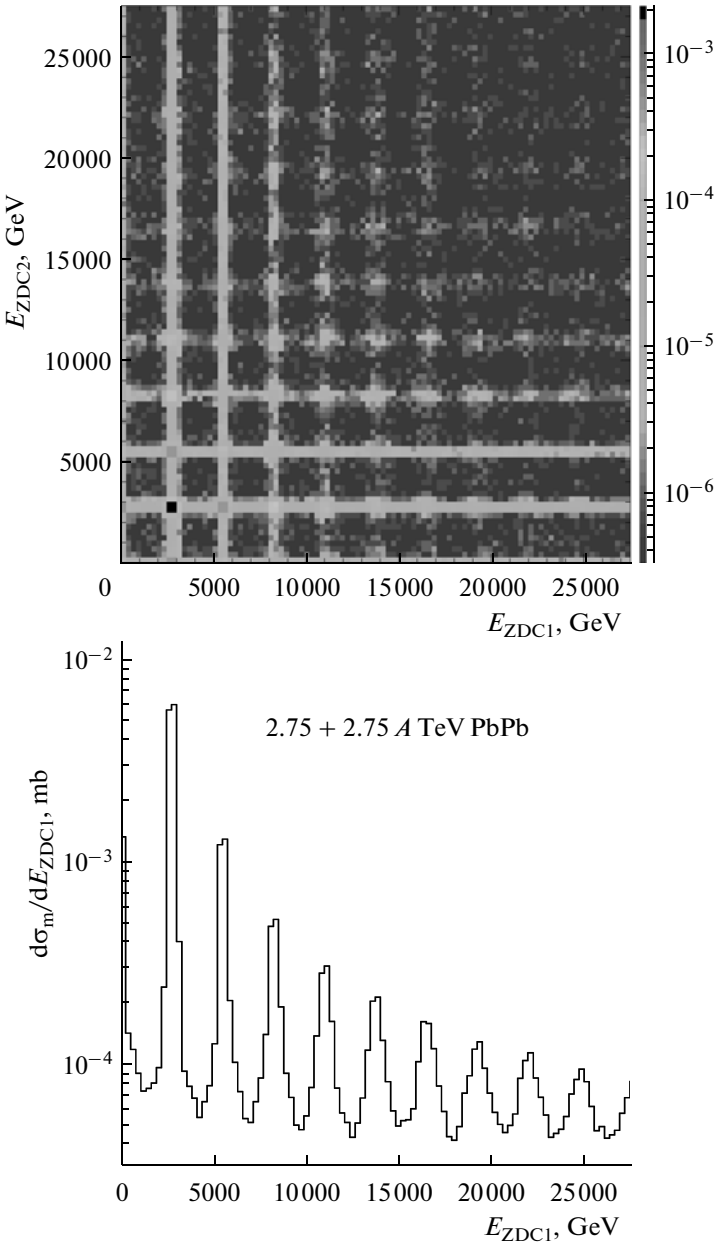

Fig. 19. Upper panel: correlations of total energies registered in each of the ZDCs in events of mutual dissociation of lead nuclei at the LHC. Lower panel: energy distribution in a ZDC obtained by projecting an upper distribution. Distributions are calculated for the leading order and do not take into account ZDC hardware resolution [14].

It is seen from Table 10 that the uncertainty ~10% is present in the quantity $\sigma(1nX|1nY)$ resulting from uncertainties in photonuclear reactions. Nevertheless, the uncertainty $\sigma^{MED}(LMN)$ is estimated to be of the order of ~2%. The quantity $\sigma^{MED}(LMN)$ is also more stable with respect to variations in calculation parameters; therefore, it can be recommended for monitoring the LHC luminosity, just as at the RHIC (see Subsection 5.1).

At the LHC energies, the GR excitation in both colliding nuclei under mutual impact of their Coulomb fields is not the only process leading to neutron loss in the nuclei. Therefore, asymmetric events with electromagnetic excitations of nuclei are possible in which GR excitation in one nucleus is accompanied by photonuclear reactions in another nucleus occurring under the impact of more energetic photons. Figure 19 shows the presence of such asymmetric dissociation processes that manifest themselves in correlations between total energies detected by each ZDC.

The ZDCs to be used in the ALICE experiment at the LHC have certain advantages over analogous detectors installed at the RHIC. At the LHC, the resolution in neutron energies detected by ZDC is

expected to be around ~10% [9], whereas at the RHIC it is ~20% [97]. This allows one to expect that $3n$ and $4n$ channels will successfully be identified at the LHC, thereby opening to researchers the rich world of multiple excitations of giant resonances.

6. CONCLUSIONS

The study of ultraperipheral nuclear collisions is an area in which the branches of classical nuclear physics that explore the structure and collective excitations of nuclei merge with the new physics of ultrarelativistic nuclear interactions. An approach to electromagnetic nuclear interactions discussed above and implemented in the RELDIS computer model successfully describes a large set of experimental data obtained in experiments with both fixed targets and colliding beams, with the latter conducted at the RHIC.

A successful description of existing RHIC experimental data by the RELDIS model justifies applications of this model to predict the characteristics of electromagnetic dissociation of nuclei at the LHC collider that will soon be used for studying nuclear collisions. It should be emphasized that, despite all the achievements of the theory of electromagnetic nuclear dissociation, further development of this approach is still required. First, a consistent quantum-mechanical description of microscopic properties of multiphoton excitations in giant resonances in the collisions of ultrarelativistic nuclei should be developed so as to search for those specific channels of their decay that will be convenient for experimental identification. Second, it is necessary to study the possible impact of nuclear Coulomb fields exerted upon the characteristics of peripheral hadronic interactions of nuclei, since electromagnetic and nuclear forces act simultaneously in every event. In particular, these lines of theory development are important for describing collisions of light nuclei, in which the microscopic structure of GR should reveal itself and the role played by incoherent processes of equivalent photon emission increases relative to coherent ones.

ACKNOWLEDGMENTS

I would like to thank my coauthors of original works dedicated to electromagnetic dissociation of nuclei for long-term fruitful cooperation and support. I am indebted to I.N. Mishustin, J. Bondorf, A.S. Botvina, A.S. Iljinov, A.B. Kurepin, A. Ventura, C. Scheidenberger, K. Sümmerer, H. Braun, J.M. Jowett, U. Uggerhöj, and A. Morsch, just to name a few. I am also grateful to A. Baltz, S. White, and M. Strikman for numerous discussions of ultraperipheral nuclear collisions.

REFERENCES

1. G. Baym, Nucl. Phys. A **698**, 23 (2002).
2. A. G. Litvinenko, Fiz. Elem. Chastits At. Yadra **38**, 409 (2007) [Phys. Part. Nucl. **38**, 204 (2007)].
3. R. G. de Cassagnac, Int. J. Mod. Phys. A **22**, 6043 (2007).
4. C. L. Timoshenko and V. M. Emel'yanov, Fiz. Elem. Chastits At. Yadra **37**, 1150 (2006) [Phys. Part. Nucl. **37**, 606 (2006)].
5. L. Evans, New J. Phys. **9**, 335 (2007).
6. P. Cortese et al. (ALICE Collab.), J. Phys. G: Nucl. Part. Phys. **30**, 1517 (2004).
7. B. Alessandro et al. (ALICE Collab.), J. Phys. G: Nucl. Part. Phys. **32**, 1295 (2006).
8. C. Adler, A. Denisov, E. Garcia, M. Murray, H. Stroebele, and S. White, Nucl. Instrum. Methods Phys. Res. A **461**, 488 (2001).
9. C. Oppedisano, "Centrality Measurement in the ALICE Experiment with the Zero Degree Calorimeters," ALICE Internal Note, ALICE-INT-2002-08 (2002).
10. G. Puddu, R. Arnaldi, E. Chiavassa, et al., Nucl. Instrum. Methods Phys. Res. A **581**, 397 (2007).
11. F. Krauss, M. Greiner, and G. Soff, Prog. Part. Nucl. Phys. **39**, 503 (1997).
12. G. Baur, K. Hencken, and D. Trautmann, J. Phys. G **24**, 1657 (1998).
13. G. Baur, K. Hencken, D. Trautmann, S. Sadovsky, and Y. Kharlov, Phys. Rep. **364**, 359 (2002).
14. A. J. Baltz, G. Baur, D. d'Enterria, et al., Phys. Rep. **458**, 1 (2008).
15. C. A. Bertulani and G. Baur, Phys. Rep. **163**, 299 (1988).
16. V. G. Nedorezov and Yu. N. Ranyuk, Fiz. Elem. Chastits At. Yadra **15**, 379 (1984) [Sov. J. Part. Nucl. **15**, 172 (1984)].
17. J. Eisenberg and W. Greiner, *Nuclear Models* (North-Holland, Amsterdam, 1988; Atomizdat, Moscow, 1975).
18. B. S. Ishkhanov and V. N. Orlin, Fiz. Elem. Chastits At. Yadra **38**, 460 (2007) [Phys. Part. Nucl. **38**, 232 (2007)].
19. P. S. Isaev, *Quantum Electrodynamics at High Energies* (Energoatomizdat, Moscow, 1984; Amer. Inst. Physics, New York, 1989).
20. V. G. Nedorezov, A. A. Turinge, and Yu. M. Shatunov, Usp. Fiz. Nauk **174**, 353 (2004) [Phys. Usp. **47**, 341 (2004)].
21. R. Palit, P. Adrich, T. Aumann, et al., Phys. Rev. C **68**, 034318 (2003).
22. C. A. Bertulani and V. Yu. Ponomarev, Phys. Rep. **321**, 139 (1999).
23. T. Aumann, P. F. Bortignon, and H. Emling, Ann. Rev. Nucl. Part. Sci. **48**, 351 (1998).
24. K. Boretzky, A. Grunschloss, S. Ilievski et al., Phys. Rev. C **68**, 024317 (2003)
25. C. A. Bertulani, L. F. Canto, and M. S. Hussein, Phys. Rep. **226**, 281 (1993).
26. A. Heinz, K. H. Schmidt, A. R. Junghans, et al., Nucl. Phys. A **713**, 3 (2003)
27. J. P. Bondorf, A. S. Botvina, A. S. Iljinov, I. N. Mishustin, and K. Sneppen, Phys. Rep. **257**, 133 (1995).

28. A. J. Baltz, M. J. Rhoades-Brown, and J. Weneser, Phys. Rev. C **54**, 4233 (1996).
29. S. R. Klein, Nucl. Instrum. Methods Phys. Res. A **459**, 51 (2001).
30. I. A. Pshenichnov, I. N. Mishustin, J. P. Bondorf, A. S. Botvina, and A. S. Iljinov, Phys. Rev. C **57**, 1920 (1998).
31. I. A. Pshenichnov, I. N. Mishustin, J. P. Bondorf, A. S. Botvina, and A. S. Iljinov, Phys. Rev. C **60**, 044901 (1999).
32. I. A. Pshenichnov, J. P. Bondorf, I. N. Mishustin, A. Ventura, and S. Masetti, Phys. Rev. C **64**, 024903 (2001).
33. J. D. Jackson, *Classical Electrodynamics*, 2nd ed. (Wiley, New York, 1975).
34. E. Fermi, Nuovo Cim. **2**, 143 (1925).
35. E. Fermi, "On the Theory of Collisions between Atoms and Electrically Charged Particles," arXiv:hep-th/0205086.
36. C. F. von Weizsacker, Z. Phys. **88**, 612 (1934).
37. E. J. Williams, Phys. Rev. **45**, 729 (1934).
38. A. S. Iljinov, I. A. Pshenichnov, N. Bianchi, E. de Sanctis, V. Muccifora, M. Mirazita, and P. Rossi, Nucl. Phys. A **616**, 575 (1997).
39. I. A. Pshenichnov, B. L. Berman, W. J. Briscoe, C. Cetina, G. Feldman, P. Heimberg, A. S. Iljinov, and I. I. Strakovsky, Eur. J. Phys. A. **24**, 69 (2005).
40. P. Golubev, V. Avdeichikov, K. G. Fissum, B. Jakobsson, I. A. Pshenichnov, et al., Nucl. Phys. A **806**, 216 (2008).
41. V. S. Barashenkov, F. G. Gereghi, A. S. Iljinov, G. G. Jonsson, and V. D. Toneev, Nucl. Phys. A **231**, 462 (1974).
42. A. S. Botvina, A. S. Iljinov, I. N. Mishustin, J. P. Bondorf, R. Donangelo, and K. Sneppen, Nucl. Phys. A **475**, 663 (1987).
43. A. Veyssière, H. Beil, R. Bergère, P. Carlos, and A. Leprêtre, Nucl. Phys. A **159**, 561 (1970).
44. J. S. Levinger, Phys. Rev. **84**, 43 (1951).
45. A. Leprêtre, H. Beil, R. Bergère, P. Carlos, J. Fagot, A. De Miniac, and A. Veyssière, Nucl. Phys. A **367**, 237 (1981).
46. J. M. Laget, Nucl. Phys. A **312**, 265 (1978).
47. C. Guaraldo, V. Lucherini, E. De Sanctis, A. S. Iljinov, M. V. Mebel, and S. Lo Nigro, Nuovo Cim. A **103**, 607 (1990).
48. A. Leprêtre, H. Beil, R. Bergère, P. Carlos, J. Fagot, A. De Miniac, and A. Veyssière, Nucl. Phys. A **390**, 221 (1982).
49. W. J. Llope and P. Braun-Munzinger, Phys. Rev. C **41**, 2644 (1990).
50. B. L. Berman and B. L. Fultz, Rev. Mod. Phys. **47**, 713 (1975).
51. S. S. Dietrich and B. L. Berman, At. Data Nucl. Data Tables. **38**, 199 (1988).
52. M. Mirazita, H. Avakian, N. Bianchi, A. Deppman, E. De Sanctis, V. Gyurjyan, V. Muccifora, E. Polli, P. Rossi, R. Burgwinkel, J. Hannappel, F. Klein, D. Menze, W. Schwille, and F. Wehnes, Phys. Lett. B **407**, 225 (1997).
53. V. Muccifora, N. Bianchi, A. Deppman, E. De Sanctis, M. Mirazita, E. Polli, P. Rossi, R. Burgwinkel, J. Hannappel, F. Klein, D. Menze, W. J. Schwille, and F. Wehnes, Phys. Rev. C **60**, 064616 (1999).
54. N. Bianchi, E. De Sanctis, M. Mirazita, and V. Muccifora, Phys. Rev. C **60**, 064617 (1999).
55. R. R. Harvey, J. T. Caldwell, R. L. Bramblett, and S. C. Fultz, Phys. Rev. **136**, B126 (1964).
56. B. L. Berman, R. E. Pywell, S. S. Dietrich, M. N. Thompson, K. G. McNeill, and J. W. Jury, Phys. Rev. C **36**, 1286 (1987).
57. R. Engel, J. Ranft, and S. Roesler, Phys. Rev. D **55**, 6957 (1997).
58. A. J. Baltz, C. Chasman, and S. N. White, Nucl. Instrum. Methods Phys. Res. A **417**, 1 (1998).
59. J. D. T. Arruda-Neto, S. Simionatto, V. P. Lichachev, F. Garcia, J. Mesa, A. Deppman, O. Rodriguez, and F. Guzmàn, Nucl. Phys. **638**, 701 (1998).
60. E. Wolynec, A. R. V. Martinez, P. Gouffon, Y. Miyao, V. A. Serrao, and M. N. Martins, Phys. Rev. C **29**, 1137 (1984).
61. S. N. Whight, Nucl. Instrum. Methods Phys. Res. A **409**, 618 (1998).
62. S. N. Belyaev and V. A. Semenov, Izv. RAN, Ser. Fiz. **55**, 953 (1991).
63. V. V. Varlamov, N. G. Efimkin, B. S. Ishkhanov, and V. V. Sapunenko, Yad. Konst. **1**, 52 (1993).
64. P. G. Young, E. D. Arthur, and M. B. Chadwick, in *Nuclear Reaction Data and Nuclear Reactors, Physics, Design and Safety*, Lecture Series 1996, Trieste, Italy, Ed. by A. Gandini and G. Reffo (World Sci., Singapore, 1998), vol. 1, p. 227.
65. M. B. Chadwick and P. G. Young, Acta Phys. Slovaca **45**, 633 (1995).
66. M. B. Chadwick, P. Obložinsky, G. Reffo, and P. E. Hodgson, Phys. Rev. C **44**, 814 (1991).
67. A. M. van den Berg, D. Chmielewska, J. A. Bordewijk, S. Brandenburg, A. van der Woude, Y. Blumenfeld, N. Frasaria, J. C. Roynette, J. A. Scarpaci, T. Suomijärvi, N. Alamados, F. Auger, A. Gillibert, P. Roussel-Chomaz, J. Blomgren, L. Nilsson, N. Olsson, and R. Turcotte, Nucl. Phys. A **578**, 238 (1994).
68. R. Alarcon, P. L. Cole, D. S. Dale, P. T. Debevec, and L. J. Morford, Phys. Rev. C **43**, R2470 (1991).
69. R. F. Askew and A. P. Batson, Nucl. Phys. **20**, 408 (1960).
70. F. Tagliabue and J. Goldemberg, Nucl. Phys. **23**, 144 (1961).
71. G. A. Chekomazov and M. H. Urin, Phys. Lett. B **354**, 7 (1995).
72. J. C. Hill, A. Petridis, B. Falem, and F. K. Wohn, Nucl. Phys. A **661**, 313 (1999).
73. M. B. Golubeva, F. F. Guber, T. L. Karavicheva, E. V. Karpechev, A. B. Kurepin, A. I. Maevskaya, I. A. Pshenichnov, et al., Phys. Rev. C **71**, 024905 (2005).
74. H. Dekhissi, G. Giacomelli, M. Giorgini, G. Mandrioli, S. Manzoor, L. Patrizii, V. Popa, P. Serra, and V. Togo, Nucl. Phys. A **662**, 207 (2000).

75. C. Scheidenberger, I. A. Pshenichnov, K. Summerer, A. Ventura, J. P. Bondorf, A. S. Botvina, et al., Phys. Rev. C **70**, 014902 (2004).
76. C. Scheidenberger, I. A. Pshenichnov, T. Aumann, S. Datz, K. Summerer, Bondorf J. P. et al., Phys. Rev. Lett. **88**, 042301 (2002).
77. C. H. Tsao, R. Silberberg, and A. F. Barghouty, Astrophys. J. **501**, 920 (1998).
78. L. Y. Geer, J. Klarmann, B. S. Nilsen, C. J. Waddington, W. R. Binns, J. R. Cummings, and T. L. Garrard, Phys. Rev. C **52**, 334 (1995).
79. K. Sümmerer, J. Reinhold, M. Fauerbach, J. Friese, H. Geissel, H. J. Körner, G. Münzenberg, R. Schneider, and K. Zeitelhack, Phys. Rev. C **52**, 1106 (1995).
80. J. R. Cummings, W. R. Binns, T. L. Garrard, M. H. Israel, J. Klarmann, E. C. Stone, and C. J. Waddington, Phys. Rev. C **42**, 2508 (1990).
81. C. J. Waddington, J. R. Cummings, B. S. Nilsen, and T. L. Garrard, Phys. Rev. C **61**, 024910 (2000).
82. S. E. Hirzebruch, E. Becker, G. Hüntrup, T. Streibel, E. Winkel, and W. Heinrich, Phys. Rev. C **51**, 2085 (1995).
83. C. A. Bertulani and D. S. Dolci, Nucl. Phys. A **674**, 527 (2000).
84. G. Baur, K. Hencken, A. Aste, D. Trautmann, and S. R. Klein, Nucl. Phys. A **729**, 787 (2003).
85. C. J. Benesh and J. L. Friar, Phys. Rev. C **50**, 3167 (1994).
86. K. Hencken, D. Trautmann, and G. Baur, Phys. Rev. C **53**, 2532 (1996).
87. K. Hencken, D. Trautmann, and G. Baur, Z. Phys. C **68**, 473 (1995).
88. T. Aumann, C. A. Bertulani, and K. Summerer, Phys. Rev. C **51**, 416 (1995).
89. C. J. Benesh, B. C. Cook, and J. P. Vary, Phys. Rev. C **40**, 1198 (1989).
90. A. Grunschloss, K. Boretzky, T. Aumann, et al., Phys. Rev. C **60**, 051601 (1999).
91. J. Hüfner, K. Schäfer, and B. Schürmann, Phys. Rev. C **12**, 1888 (1975).
92. H. Emling, Prog. Part. Nucl. Phys. **33**, 729 (1994).
93. E. J. V. de Passos, M. S. Hussein, L. F. Canto, and B. V. Carlson, Phys. Rev. C **65**, 034326 (2002).
94. M. Chiu, A. Denisov, E. Garcia, J. Katzy, and S. White, Phys. Rev. Lett. **89**, 012302 (2002)
95. H.-H. Braun, R. W. Assmann, A. Ferrari, J.-B. Jeanneret, J. M. Jowett, and I. A. Pshenichnov, in *Proceedings of the 9th European Particle Accelerator Conference, Lucerne, Switzerland, 5–9 July 2004*, p. 551.
96. J. M. Jowett, H.-H. Braun, M. I. Gresham, E. Mahner, A. N. Nicholson, E. N. Shaposhnikova, and I. A. Pshenichnov, in *Proceedings of the 9th European Particle Accelerator Conference, Lucerne, Switzerland, 5–9 Jul 2004*, p. 578.
97. C. Adler, H. Strobele, A. Denisov, E. Garcia, M. Murray, and S. White, Nucl. Instrum. Methods Phys. Res. A **461**, 337 (2001).